SAE Paper 2004-01-2936

# Molecular Structure Effects On Laminar Burning Velocities At Elevated Temperature And Pressure

**J. T. Farrell, R. J. Johnston, and I. P. Androulakis**
ExxonMobil Research and Engineering



## ABSTRACT

The laminar burning velocities of 45 hydrocarbons have been investigated in a constant volume combustion vessel at elevated temperature and pressure. The mixtures are ignited in the center of a spherical vessel at an initial temperature of 450 K and pressure of 304 kPa. Data have been acquired over the stoichiometry range of $0.55 \leq \phi \leq 1.4$. The burning velocity is determined from a thermodynamic analysis of the pressure vs. time data. The results for alkanes and alkenes are consistent with trends previously identified in the literature, i.e., alkenes are faster than the corresponding alkane with the same carbon connectivity. For both alkanes and alkenes, branching lowers the burning velocity. In addition, terminal alkenes and alkynes are found to be slightly faster than internal alkenes and alkynes. The present study includes broader coverage of aromatics than previous literature reports. The burning velocities for aromatics show a strong dependence on the type and site of alkyl substitution; methyl substitution lowers the burning velocity more than substitution with larger alkyl groups. For multiple methyl group substitution, meta substitution lowers the burning velocity more than ortho/para. The physical and chemical kinetic bases for the variation of burning velocity with molecular structure are discussed with the aid of elemental flux analyses of simulations using detailed chemical kinetic mechanisms. A consistent trend is identified in which "fast" burning fuels have a higher flux into decomposition pathways that yield H atoms and $C_2$ fragments, while "slow" fuels have a higher flux into pathways that form $CH_3$ radicals. The data and analysis presented in this paper provide a comprehensive, fundamental basis for relating fuel structure effects to combustion efficiency and emissions.

## INTRODUCTION

Laminar burning velocities for hydrocarbons have long been the subject of extensive experimental and theoretical investigation. This interest in part reflects the important role of the burning velocity in the performance of spark-ignition engines [1]. For example, the fuel's burning velocity affects the burn rate in the engine and therefore its efficiency [2] and emissions. On a more fundamental level, the burning velocity depends only on the mixture composition, temperature, and pressure, and is thus a fundamental property of a combustible mixture. This makes it an important target for combustion modeling, in particular the validation of kinetic mechanisms.

Even though much experimental and modeling work on burning velocities has been reported, a quantitative understanding of molecular structure effects is still incomplete. Since the 1950s a substantial amount of experimental data has been collected for a wide range of $C_1$-$C_8$ molecules [3-20]. As discussed by Andrews and Bradley [21], however, significant discrepancies were often observed between the burning velocities obtained from the earlier measurements, which utilized experimental techniques such as Bunsen burners, open tubes, and constant volume vessels. It is now understood [21,22] that these discrepancies are due to the presence of varying degrees of flame curvature and aerodynamic strain - collectively denoted "stretch" - which contributed significantly to the large amount of scatter in the literature data. Careful studies during the past two decades have quantified the effects of stretch and have shown that the intrinsic stretch-free burning velocities can be determined with a number of experimental techniques, such as counter flow axisymmetric burners and constant volume combustion chambers [9,13,22]. Unfortunately, data for only a limited range of fuels have been reported with these techniques.

Although it is difficult to carry out quantitative comparisons of these earlier data to detailed models, these results have permitted the development of empirical relationships [23] and group additivity [24] approaches to predicting burning velocities. In addition, they have served the important practical purpose of providing information on relative fuel effects. For alkanes, alkenes, and alkynes, there is a general consensus on how fuel structure affects burning velocity. For example,

alkynes and other highly unsaturated species have fast burning velocities. Alkenes are generally slower than alkynes but faster than the corresponding alkane, i.e., the alkane with the same carbon connectivity (e.g., iso-butene vs. iso-butane). In addition, branched alkenes and alkanes are slower than the unbranched analogues. When compared at equivalent pressure and unburned gas temperature, these effects reflect differences due to burned gas temperature and kinetics. For aromatics, no clear consensus exists, mostly due to the lack of experimental studies and inconsistencies in the literature. In general, benzene is acknowledged as the fastest burning aromatic. While substitution decreases the burning velocity, the dependence on type and site of alkyl substitution is incompletely understood.

Extending this qualitative understanding to a more quantitative level requires analyses using detailed elementary chemical kinetic mechanisms. While such analyses have been performed for several prototypical systems [25-28], extension to larger fuels has historically been limited by the unavailability of the requisite detailed kinetic mechanisms, though there has been recent progress in this area [29-31].

The purpose of the present paper is to characterize the laminar burning velocities of a wide range of hydrocarbons over a broad stoichiometry range at elevated temperature and pressure. The emphasis has been to determine relative fuel effects for alkanes, alkenes, alkynes, aromatics, and oxygenates under equivalent experimental conditions. The measurements are carried out in a constant volume combustion vessel with both pressure-based and high-speed schlieren visualization diagnostics. Validation data are reported for $CH_4$, $C_2H_6$, and $C_4H_{10}$ under ambient conditions (T=300K, P=101 kPa). The discussion of molecular structure effects on laminar burning velocities is an extension of that from Davis and Law [7]. This analysis involves separate consideration of the effects of extensive properties (temperature and pressure) and kinetic factors. The discussion of aromatics, in particular, is more comprehensive than earlier reports. Blending effects will be the subject of future investigations, as will the determination of Markstein lengths and identification of combustion instabilities for select fuels.

## EXPERIMENTAL

A schematic of the experimental apparatus is shown in Figure 1. The stainless steel vessel has a 16.5 cm diameter spherical cavity (volume = 2.4 liter) with four windows for optical access. The two largest are 7.6 cm sapphire windows (6.4 cm clear aperture) arranged on opposite sides of the vessel which allow the transmittance of a collimated light beam for schlieren diagnostics. Perpendicular to these windows is a smaller sapphire window (6.4 cm diameter; 5.1 cm clear aperture) which admits the laser ignition pulse. A fourth sapphire window (3.2 cm diameter; 2.5 cm aperture) is located at the top of the vessel and provides optical access for an intensified UV CCD camera (not used in the present investigation). The vessel is housed in a temperature-controlled oven capable of maintaining a constant temperature to within ~1-2 °C over an extended time period (weeks). The oven has quartz windows to allow transmission of the optical beams.

Fuel/air mixtures are prepared by charging the vessel with the hydrocarbon to the pressure required for the desired mixture stoichiometry. Fuels that are gaseous under ambient conditions are charged directly from lecture bottles through mass flow controllers. Liquid fuels are first vaporized in a heated, evacuated 11-liter chamber and then charged through heated lines into the vessel. A schematic of the gas delivery system is also shown in Figure 1. The air charge is admitted next until the desired pressure is achieved. A high sensitivity MKS Baratron (10,000 Torr = 1.3 MPa range) is used to monitor the fuel and air pressure during charging of the vessel. Computerized control of the gas delivery is used to maintain precise control over the mixture composition. The gas is allowed to equilibrate for several minutes. Prior to ignition, a valve is closed to prevent damage to the Baratron from the rapid pressure rise. For most of the fuels, ignition is initiated in the center of the vessel by means of laser-induced breakdown achieved with the focused output of a single Nd:YAG laser pulse (Spectra Physics GCR-250-10, 532 nm). The ignition energy is typically ~10-50 mJ/pulse, and is adjusted to be just above the minimum ignition energy to avoid deposition of excess energy into the mixture. The ignition pulse is initially collimated to a diameter of ~ 15 mm with a

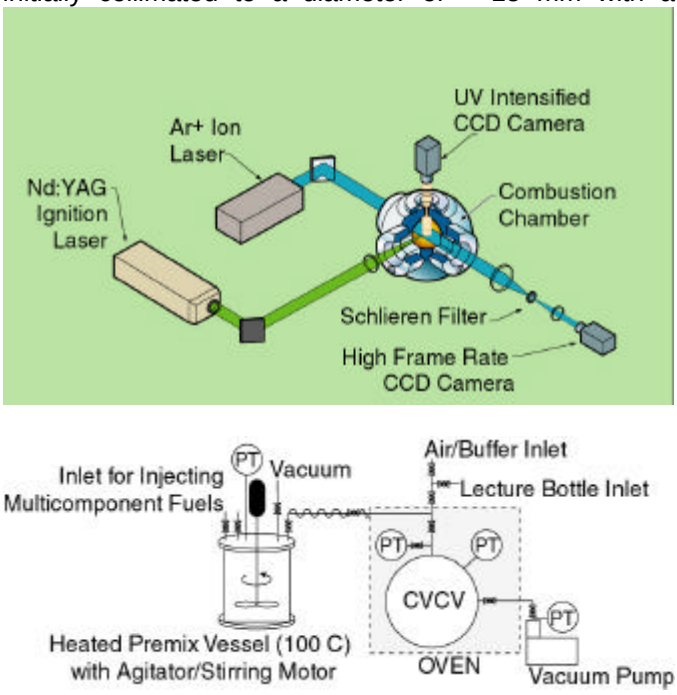


Figure 1: Schematic of Experimental Apparatus

telescope after which it is focused into the center of the vessel with a fused silica lens (ϕ=25 mm, f.l. = 125 mm). Laser-induced breakdown of air is used to visually center the beam waist in the vessel.

Alternatively, results are presented for several fuels in which ignition was effected with an electrical discharge across a pair of tungsten electrodes. As will be shown below, nearly equivalent results are obtained with both ignition techniques. Following ignition, the pressure rise in the vessel is monitored with a fast, high dynamic range pressure transducer (Kistler 6051B). The transducer output is conditioned, digitized, and transferred to a personal computer for analysis. Video data acquisition is also triggered by the laser pulse.

In addition to the pressure rise data, high-speed visualization data have been acquired for a small number of fuels using schlieren photography. The schlieren light source is either a small frame, air-cooled argon ion laser (Ion Laser Technology 5500A) or a mercury discharge lamp (Leitz). The beam is expanded to 2.5" diameter and collimated, after which it passes through quartz oven windows and the sapphire windows of the vessel. The transmitted light is then focused with a lens (3.0" diameter, 300 mm focal length). An apodizing filter (Reynard Corporation) is placed in the focal plane of this lens to attenuate the undeviated light rays. A Redlake Motionscope 8000S camera, placed behind the apodizing filter, is used to acquire the schlieren images at 2000 frames per second.

The fuels investigated in this study are listed in Table 1. The gaseous fuels ($C_1$-$C_4$ alkanes, alkenes, and alkynes) were used directly from lecture bottles without further purification. The stated purities of the gases were 96.5-99.99%. The liquid fuels (Aldrich Chemical) have the purities listed in Table 1 and were also used without further purification.

## RESULTS AND ANALYSIS

The burning velocity data are derived from a thermodynamic analysis of the pressure rise following ignition. Figure 2 shows vessel pressure vs. time data for methylcyclopentane at 450 K and 304 kPa over the equivalence ratio range $0.55 \le \phi \le 1.30$. Multiple (~2-3) measurements are recorded for each fuel at each stoichiometry to reduce statistical uncertainty. As shown in the figure, the repeatability of the data is very high, reflecting precise control over mixture composition.

The thermodynamic analysis of the pressure vs. time data follows the approach of Metghalchi and Keck [14,15]. Conservation of mass, energy, and volume are invoked via the following equations:

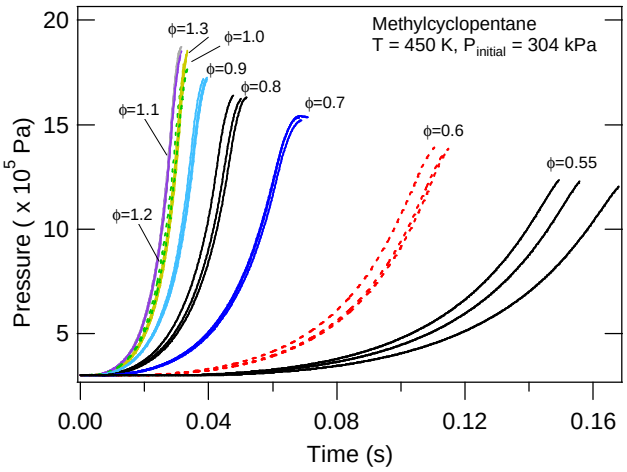


Figure 2: Pressure vs. time data for methylcyclopentane mixtures over the equivalence ratio (ϕ) range $0.55 \le \phi \le 1.30$.

$$M = m_u + m_b = \frac{p}{R}\left(\frac{V_u W_u}{T_u} + \frac{V_b W_b}{T_b}\right) \quad \text{(Eq. 1)}$$

$$E = Me = m_u e_u(T_u) + m_b e_b(T_b) \quad \text{(Eq. 2)}$$

$$V_C = V_u + V_b \quad \text{(Eq. 3)}$$

The equation for isentropic compression of the unburned gas mixture is

$$\int_{T_0}^{T_{u,i}} \frac{C_{p,u}}{T}dT - \int_{p_0}^{p_i} \frac{R}{pW_u}dp = \int_{T_0}^{T_u} \frac{C_{p,u}}{T}dT - \int_{p_0}^{p} \frac{R}{pW_u}dp \quad \text{(Eq. 4)}$$

where

$M, m_u, m_b$ = total mass, mass of unburned gas, and mass of burned gas in combustion chamber

$E, e, e_u, e_b$ = total energy, energy per unit mass, energy of unburned gas, and energy of burned gas of gas in combustion chamber

$V_c, V_u, V_b$ = volume of combustion chamber, unburned gas, and burned gas

p = pressure

$T_c, T_u, T_b$ = temperature, unburned gas temperature, and burned gas temperature

$W_u, W_b$ = molecular weight of unburned and burned gas

Table 1: Fuels investigated in this study and their associated purities

| **Alkanes** | Purity |
|---|---|
| methane | 99.99% |
| ethane | 99.99% |
| propane | 99% |
| n-butane | 99% |
| iso-butane | 99% |
| n-pentane | 99+% |
| 2-methylbutane (iso-pentane) | 99+% |
| 2,2-dimethylpropane (neopentane) | 99.5% |
| cyclopentane | 99+% |
| n-hexane | 99+% |
| methylcyclopentane | 99+% |
| cyclohexane | 98% |
| n-heptane | 99+% |
| 2,2,4-trimethylpentane (iso-octane) | 99+% |
| | |
| **Aromatics** | |
| benzene | 99.8% |
| toluene | 99.8% |
| o-xylene | 98% |
| m-xylene | 99+% |
| p-xylene | 99+% |
| ethylbenzene | 99.8% |
| n-propylbenzene | 98% |
| iso-propylbenzene | 99% |
| 1,2,4-trimethylbenzene | 98% |
| 1,3,5-trimethylbenzene | 97% |
| t-butylbenzene | 99% |

| **Alkenes/Alkynes** | Purity |
|---|---|
| ethylene | 99.99% |
| propylene | 99% |
| allene | 96.5%* |
| 1-butene | 99% |
| 2-butene | 99% |
| 1-butyne | 99% |
| 2-butyne | 99% |
| 1-pentene | 99% |
| 2-pentene | 99% |
| 2-methyl-1-butene | 96% |
| 2-methyl-2-butene | 99+% |
| cyclopentene | 99.5% |
| 1-hexene | 99+% |
| 1-heptene | 99+% |
| 3-heptene | 99% |
| 1-octene | 98% |
| 2,4,4-trimethyl-1-pentene (iso-octene) | 99% |
| | |
| **Oxygenates** | |
| ethanol | 99+% |
| methyl-t-butyl ether (MTBE) | 99+% |
| methoxy benzene (anisole) | 99.7% |

* allene impurities = cyclopropane (2.3%), propylene (0.8%), propane (0.2%), and propyne (0.1%)

R = universal gas constant

$C_{p,u}$ = specific heat at constant pressure of unburned gas

At each time step, the pressure is used to calculate the isentropically compressed unburned gas temperature. Unburned gas properties are computed using thermodynamic data from either the JANAF tables [32] or an ExxonMobil thermodynamic compilation [33]. The mass fraction burned ($x = m_b/(m_u+m_b)$) is then determined based on an estimated burned gas temperature $T_b$. The corresponding equilibrium burned gas composition and burned gas thermodynamic properties are calculated. The burned composition is determined using a program adopted from Strehlow [34] and the burned gas thermodynamic properties are estimated using the approach outlined by Heywood [35]. Conservation of energy is used to iteratively refine the value for $T_b$, and the revised value for x is used to calculate the total mass burned $m_b$. This procedure is repeated at each pressure step. The mass burn rate $dm_b/dt$ is calculated via a linear least squares fit. The laminar burning velocity is then computed using the definition

$$S_u = \frac{dm_b/dt}{r_u A_f} \qquad \text{(Eq. 5)}$$

where

$dm_b/dt$ = mass burning rate

$\rho_u$ = unburned gas density

$A_f$ = flame front area = $(4/3)\pi r_f^2$

$r_f$ = flame front radius = $[3V_f/4\pi]^{1/3}$

$V_f$ = burned gas volume = $V_C - V_u$

This analysis requires a number of simplifying assumptions, including:

1. The unburned gas is initially at rest and has uniform temperature and composition

2. Charge stratification by gravity does not occur

3. The thickness of the reaction zone is negligible

4. The pressure in the vessel is uniform at each step in the combustion

5. The gas within the combustion chamber consists of a burned gas fraction x at local thermodynamic and chemical equilibrium and an unburned fraction 1-x at local thermodynamic equilibrium but with fixed chemical composition

6. After the completion of burning, the burned gas is at local thermodynamic equilibrium but stays at a chemically frozen state

7. The unburned gas ahead of the flame front is compressed isentropically

8. The burned gas mixture is well isolated, i.e., there is no heat or mass transfer between the burned and unburned fractions

9. The effects of buoyancy can be neglected

10. The flame front is smooth and spherical

11. The effects of flame stretch are negligible

Most of these assumptions have been either verified experimentally or are expected to be valid under the present experimental conditions. For example, schlieren measurements at $\phi$=0.55 for several of the slowest fuels show that the burn rates are sufficiently high to render the effects of buoyancy unimportant for all the fuels in the present study. Similarly, the time between (turbulent) mixture preparation and (quiescent) ignition is typically 1-2 minutes, during which time negligible charge stratification is expected to occur.

The assumption of negligible flame stretch, however, is decidedly not valid immediately following ignition, when the flame radius r and thickness $\delta$ are commensurate. This is the basis for the analysis of the unstretched burning velocity and Markstein number via schlieren visualization of the initially expanding flame [9,16,18]. However, it has been argued that by the time the flame grows to a size sufficient to register a measurable pressure rise in the vessel, the flame radius is sufficiently large ($r << \delta$) that stretch effects can be neglected [19]. Consequently, the burning velocities derived from pressure measurements are assumed to be unaffected by curvature.

***Effects of Combustion Instabilities***

The assumption of a smooth and spherical flame front is also conditional, depending on the mode of ignition and the Lewis and Markstein numbers of the mixture. Schlieren records show that laser ignition gives rise to a highly turbulent flame kernel. For very lean mixtures, the turbulence dissipates sufficiently prior to commencement of flame propagation such that the flame fronts remain smooth and spherical until late in the combustion event when they interact with the boundary layer near the wall. For most of the near-stoichiometric (and thus faster burning) flames, the ignition turbulence does not dissipate fully and the flame fronts retain large-scale cracks as they propagate. In addition, these faster flames often develop Rayleigh-Taylor (hydrodynamic) instabilities approximately 1/3 to 1/2 way during the burn. These perturbations have only a small effect on the surface area of the flame front, however, and no burn rate acceleration has been observed concomitant with appearance of these instabilities.

The same is not true for preferential diffusion instabilities, however. For rich hydrocarbon flames, preferential diffusion instabilities are evident early in the flame front propagation. These instabilities are manifested as cellular flames, which also lead to an increase in flame surface area and can signal an increase in apparent burning velocity. Bradley and coworkers [16] have presented results from experiments at high temperature and pressure (conditions which accentuate cellular flame formation) which show a dramatic increase in burning velocity upon the transition to cellular flames. In a separate detailed schlieren study of aromatic fuels at the same conditions as the present study (T=450 K, P=304 kPa), we have observed similar acceleration under rich ($\phi$ ~ 1.2-1.4) conditions [20]. Several researchers have shown that the onset of instabilities can be delayed through substitution of a rare gas such as argon for the nitrogen buffer, which increases the mixture Lewis number [19]. This approach has not been adopted in present study. The effect of these instabilities on the reported burning velocities are discussed below.

The presence of an additional combustion instability is suggested by the pressure traces in Figure 3, which are for t-butylbenzene combustion at $\phi$ =1.0 and 1.4. It can be seen that oscillations in the pressure trace are observed at the half-way point in combustion. Similar oscillations have been observed for several fuels in the present study. It is important to note that these oscillations are not commensurate with the onset of preferential diffusion instabilities, as the flame becomes cellular shortly after ignition before the vessel measures a significant pressure rise. It is also worth mentioning that the resemblance of these oscillations to those resulting from autoignition of the unburned end gas

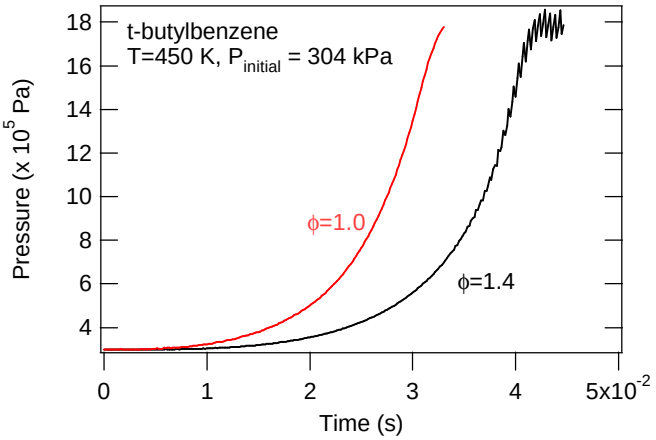


Figure 3: Pressure vs. time data for t-butylbenzene at T=450 K and P=304 kPa, showing pressure oscillations with the richer mixture commencing halfway through the pressure rise.

Identified in other constant volume combustion studies [36] is coincidental. The present oscillations result from an entirely different phenomenon as is evident by the fact that they are observed for the fuels with the highest octane numbers (most knock-resistant). They are most significant under rich conditions and large molecular weight fuels, both of which would increase the prominence of thermo-diffusive instabilities. Bradley et al. have reported similar acoustic oscillations at higher pressure with iso-octane [16,37], and Lewis and von Elbe show examples as well [38]. The oscillation frequency of 4 kHz in the present experiments is common for all fuels and commensurate with the transit time of an acoustic wave across the chamber, as observed by Bradley et al. [37].

It is well established that large hydrocarbon fuels exhibit hydrodynamic and thermo-diffusive instabilities at high temperature and pressure, and that the Markstein length decreases with increasing pressure [8]. When the flame undergoes the transition to cellular structure, the flame surface area can increase rapidly leading to an acceleration in flame speed. The corresponding pressure pulses can reflect off the walls and deform the flame by Taylor instabilities [39].

One of the advantages often cited for pressure-based experiments in constant volume combustion vessels is the ability to extract burning velocities for a wide range of unburned gas temperatures and pressures from a single experiment. These burning velocities are often fit to a functional form and used as inputs into engine simulation codes. While these burning velocities may correlate well with engine heat release, their use to infer true burning velocity values may be compromised due to the presence of flame instabilities, the presence of which is often not determined. As the present discussion shows, there is ample evidence that instabilities exert a prominent influence on flame dynamics especially at the mildly elevated temperatures and pressures of the present study, and that caution is warranted when extracting fundamental information from these data.

***Comparison to Literature and Detailed Kinetic Mechanisms***

The burning velocity vs. unburned gas temperature data show a nearly linear growth with time as the combustion progresses until near the end where boundary layer effects slow the rate of fuel consumption. A variety of functional forms can be used to extrapolate the data back to the initial conditions where comparisons between fuels can be made under equivalent conditions. In the present analyses we fit the data to the functional form

$$S_L(T_u) = S_L(450K)T_u^a \qquad \text{(Eq. 6)}$$

where $S_u$ and $\alpha$ are fitting parameters. This functional form is often used to fit the temperature dependence of laminar burning velocities [11]. Comparable results are obtained from a linear fit to the data. The fit is executed over a data range that excludes the early (noisy) and late (boundary layer influenced) data points. Since the pressure-time history of a combustion event will differ depending on the fuel and stoichiometry, a meaningful comparison between fuels at the same temperature and pressure is most straightforward if values are compared at the same initial temperature and pressure. The data reported herein are for the initial temperature of 450 K and pressure of 304 kPa. We note that there is no physical justification for assuming a linear dependence of flame speed on burning velocity, particularly when the unburned gas pressure is also changing with time. However, over the range of temperatures and pressures investigated, this relationship has proved to be robust.

Figure 4 shows burning velocities for methane recorded under ambient conditions (T=300 K, P=101 kPa) from both pressure and schlieren data. The schlieren data have been explicitly corrected for stretch effects. Also shown in the figure are results from several other literature reports of stretch-corrected measurements. While the pressure data fall within the scatter of the other measurements, they are ~ 10% higher than the schlieren results, which agree with the currently accepted values of $S_L$ = 0.36-0.38 m/s at phi=1.1 [7,8,17]. Figure 4 also shows a comparison for ethane at ambient conditions where the same trend is apparent - the burning velocities from schlieren analyses are in better agreement to other literature results. The difference between the pressure and schlieren results for ethane is also ~ 10%.

These comparisons show that at ambient conditions, our pressure-based measurements are systematically

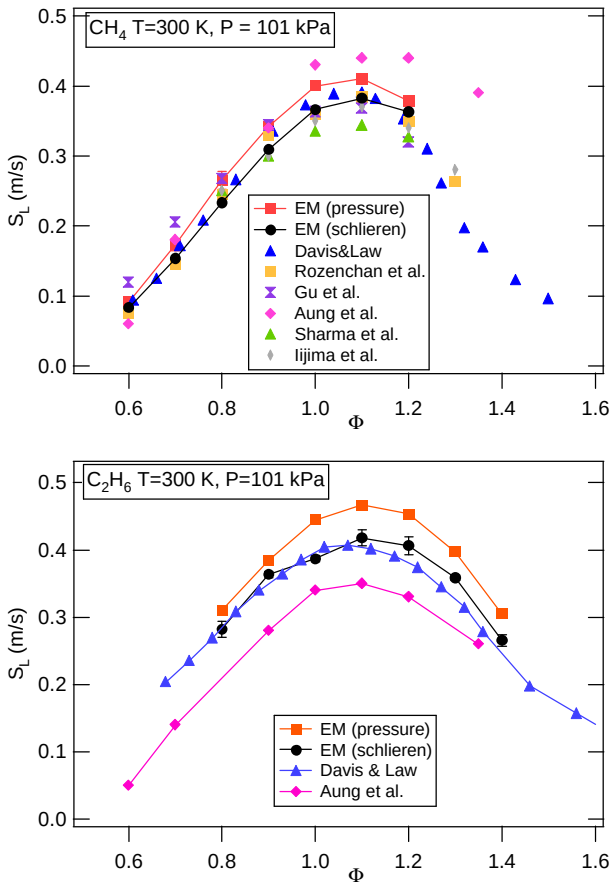


Figure 4: Laminar burning velocities of methane and ethane at T=300 K and P=101 kPa and comparison to literature data: Davis & Law [7], Rozenchan et al. [18], Gu et al. [17], Aung et al. [10], Sharma et al. [11], Iijima et al. [12]. EM refers to ExxonMobil (current measurements).

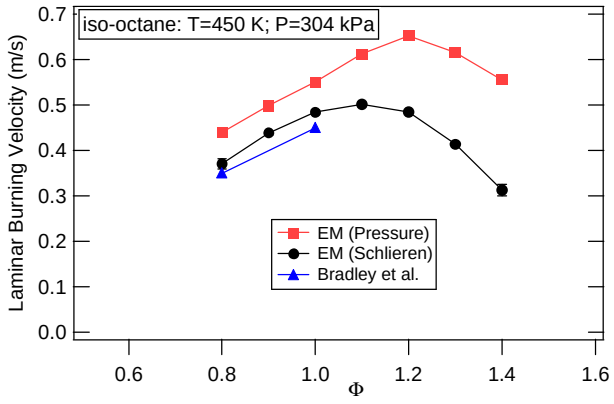


Figure 5: Laminar burning velocities of iso-octane at T=450 K and P=304 kPa and comparison to literature data from Bradley et al. [8].

slightly faster than those from flame front visualization of outwardly propagating flames or from comparison to counterflow flames. Results at the elevated T and P used in the present study are shown in Figure 5, which compares pressure and schlieren iso-octane results with the stretch-corrected values from Bradley et al. [8]. As observed under ambient conditions, the schlieren results match those of the stretch-free literature values, while the pressure results are systematically 20-30% higher. Results recently presented for aromatic fuels at the same conditions as the present study show a comparable difference [20].

There are several potential contributions to these differences. Physically, the pressure measurements record the rate of burned gas evolution rather than flame propagation rate into the cold mixture [8]. Additionally, the extrapolation method employed to determine burning velocities at the initial conditions may contribute a systematic error. Since the pressure results are consistently higher than the schlieren data, the inference of fuel structure effects on burning velocity is not affected by these differences. These differences do need to be kept in mind, however, when quantitative comparisons are made to predictions from detailed kinetic models.

***Laser vs. Electric Spark Ignition***

As mentioned above, the plasma expansion following laser-induced ignition can affect the flame front morphology and hence potentially alter the early flame chemistry. To determine whether the gas expansion following laser ignition was artificially elevating the burning velocity, several fuels were evaluated in which a spark discharge was created via an inductive discharge across tungsten needle electrodes. As shown in Figure 6, the results from both the laser and electric spark discharges are identical within the measurement repeatability. During the course of the experimental investigation, both ignition techniques were used. The data for the gaseous ($C_1$-$C_4$) fuels were collected primarily with electric discharge, while laser ignition was primarily used for the larger fuels. This reflects chronological developments in the lab rather than scientific intent. The primary reason for favoring laser vs. electric spark ignition for most of these measurements is the ability to ignite leaner mixtures with the former. However, laser ignition typically does not generate the smooth spherical flames required for schlieren analysis except for slow burning mixtures. Consequently, all the schlieren results reported herein relied on electric spark discharge.

***Summarizing Comments***

This section has discussed in detail the assumptions and methods employed in analysis of the burning velocity data. The following remarks can be made:

- Combustion instabilities (hydrodynamic and preferential diffusion) are evident in the flames, in

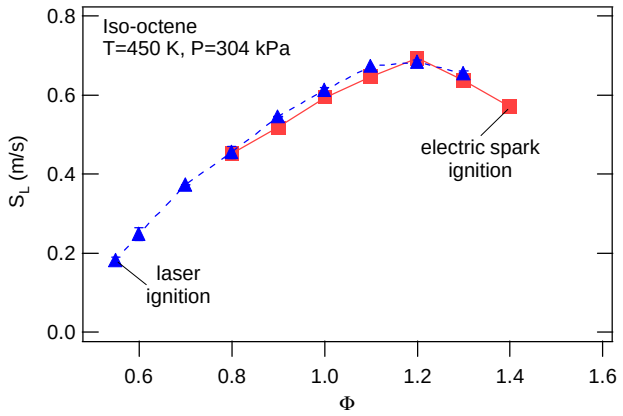


Figure 6: Burning velocities for iso-octene (2,4,4-trimethyl-1-pentene) at T=450 K and 304 kPa with both laser and electric spark ignition.

particular under near-stoichiometric and fuel-rich conditions.

- in the combustion event are most affected and least appropriate for comparison to fundamental laminar burning velocities.

- At ambient conditions, the burning velocities determined from pressure data are systematically ~ 10% higher than the stretch-free values determined from schlieren analyses. At T=450 K and P=304 kPa, the differences are ~20-30%. However, the elucidation of fuel structure effects, which is the primary purpose of this paper, is not affected by these differences.

- Comparison of electric-spark vs. laser ignition shows negligible differences.

## TIME-INTEGRATED ANALYSIS OF DETAILED KINETIC MECHANISMS

The concept of element flux analysis, introduced by Revel et al. [40], allows one to develop time-dependent flux diagrams that identify key reaction pathways with minimal effort. The principle idea is to study reaction pathways along the reaction coordinate. The atomic fluxes for each atom (C, H, O, N, Cl, etc.) at different reaction times are calculated, based on reaction rates, and the major sources and sinks for each element are identified. According to the development of Revel et al., the chemical flux of atom A from species j to species k through reaction i is defined as:

$$\dot{A}_{ijk} = q_i \frac{n_{A,j} n_{A,k}}{N_{A,i}} \qquad \text{(Eq. 7)}$$

where $q_i$ is the net production rate of reaction i, $n_{A,j}$ is the number of atoms A in species j, $n_{A,k}$ the number of atoms A in species k, and $N_{A,i}$ is the total number of atoms A in reaction i. This definition allows the atomic fluxes through a given reaction to be distributed between the different species of the reaction. In order to illustrate the definition let us consider the simple reaction:

$$CH_4 \rightarrow CH_3 + H \qquad \text{(Eq. 8)}$$

If we consider the flow of H mass, according to the definition given by (7) then we have:

$$\dot{A}_{CH_4 \rightarrow CH_3} = q \frac{4 \times 3}{8} = 3\frac{q}{2} \qquad \text{(Eq. 9a)}$$

$$\dot{A}_{CH_4 \rightarrow H} = q \frac{4 \times 1}{8} = \frac{q}{2} \qquad \text{(Eq. 9b)}$$

In equation (9), q stands for the net rate of the reaction. Here, three times more H ends up in the methyl radical than atomic H. For any given atom (A), we can then consider the transformations that occur from species to species, via all reactions in the network. The total transfer of element mass for any pair of species, as a function of time t, can then be defined as:

$$\bar{\dot{A}}_{FROM,TO}(t) = \sum_{i=1}^{N_R} \dot{A}_{i,FROM,TO}(t) \qquad \text{(Eq. 10)}$$

Where $N_R$ is the total number of reactions. The computational model used in the calculation of the quantities in (10) is a premixed plug flow reactor model. The governing equations are:

$$\frac{dy_s}{dz} = \sum_{r=1}^{N_R} \alpha_{rs} R_r, \quad \frac{dT}{dz} = \sum_{s=1}^{N_S} H_s^g \frac{dy_s}{dz}$$

$$R_r = K_r^F e^{-E_r/RT} \prod_{s=1}^{N_S} [X_s]^{\alpha'_{rs}} - K_r^R e^{-E_r/RT} \prod_{s=1}^{N_S} [X_s]^{\alpha''_{rs}}$$

$$y_s(0) = y_s^0, \quad T(0) = T^0$$

(Eq. 11)

Equation (11) defines the standard heat and material balance. Species mass fractions are denoted by y, molar concentrations are denoted by X, the stoichiometric coefficient of species s in reaction r is denoted by $\alpha_{rs}$, H is the specific enthalpy of species s, and E is the activation energy. K denotes rate constants, with the superscripts F and R denoting forward and reverse, respectively. The superscript 0 denotes initial conditions.

The thermo-physical properties and reaction rate definitions are handled using CHEMKIN [41].

Most standard stiff integrators can be used for the integration of the above systems of nonlinear ordinary differential equations. Two models have been used in the present study, a one-dimensional laminar premixed flame code [42] and a plug flow reactor (PFR) model; a more detailed discussion of the applicability of these techniques is given in Reference [43]. It has been found that for large fuels ($C_4$ and larger), the flux analyses from the PFR and laminar flame code are effectively the same. For the smaller fuels, however, notable differences are observed. Since the goal of the present investigation is to understand the pathways operative in flames, output from the flame code is used for the $C_3$ and smaller molecules.

***Time-Integrated Element Flux Analysis***

The fluxes defined in equation (10) are functions of time. Therefore, one repeats the analysis at pre-selected time instances during the reaction process. This is equivalent to taking snapshots during the reaction and trying to identify, in time, active sources and sinks. These flow charts can then be used to identify reaction pathways as they develop over time.

The approach as described makes it cumbersome to derive global information. The fluxes have to be constructed at selected points in time; however, the interval points at which these computations are performed are not always evident. We introduce in this work the concept of a time integrated flux indicator. The main idea is to derive (over time) an indicator for a source-sink combination based on integration of the quantity defined in equation (10). The quantity will be subsequently normalized as a means of representing the actual results. We, therefore, define the quantity:

$$\hat{A}_{FROM,,TO} = \frac{\int_{t=0}^{\tau} \overline{\dot{A}}_{FROM,TO}(t)\,dt}{\sum_{FROM'} \sum_{TO'} \int_{t=0}^{\tau} \overline{\dot{A}}_{FROM',TO'}(t)\,dt} \qquad \text{(Eq. 12)}$$

The integrals in equation (12) are estimated numerically by accounting for all the time instances as the integrator is selecting them. In this way, the entire reaction trajectory is taken into account and there is no need to *a priori* select the location of the snapshots. The quantity defined in (12) allows one to assign a unique, overall, number to each source-sink pair, which is representative of the entire reaction period. The normalization defined in (12) insures that pathways activated at different points in time receive appropriate weighting.

Time-integrated element flux analysis allows one to characterize the main transformations that take place during the reaction period. The analysis reveals key pathways in terms of source-sink relationships. However, this analysis does not reveal any information related to the way these transformations take place. The next step is to analyze the way these transformations take place. This is done through use of several reaction rate sensitivity methodologies. The main goal is to derive time-integrated measures that account for the global transformation during the entire reaction period.

## RESULTS

***Alkanes:***

Figure 7 shows laminar burning velocities vs. $\phi$ for methane, ethane, propane, and n-butane at T=450 K and P=304 kPa. These results and those presented hereafter are based on the thermodynamic analysis of the pressure rise data. In agreement with previous literature reports, methane has the slowest burning velocity and ethane the highest. Figure 8 shows that the burning velocities for the larger n-alkanes from propane to n-heptane are also comparable, with peak velocities of 76-78 cm/s. This relative ranking is the same as identified under ambient conditions [3,7], i.e., the burning velocities of the $C_3$ and larger linear alkanes are nearly equivalent, and intermediate between methane and ethane. The burning velocities of the branched alkanes (iso-alkanes) are also relatively independent of carbon number over the range of $C_4$-$C_8$. This is shown for iso-pentane and iso-octane in Figure 8. The peak burning velocities of the branched alkanes are roughly 15-20% slower than the normal alkane of equivalent carbon number. The burning velocities of the cycloalkanes are intermediate between the n- and iso-alkanes. The data for methylcyclopentane show that methyl substitution leads to a slight decrease in burning velocity, which directionally is consistent with the effect of branching on alkane burning velocity. These variations reflect differences in the kinetic pathways describing

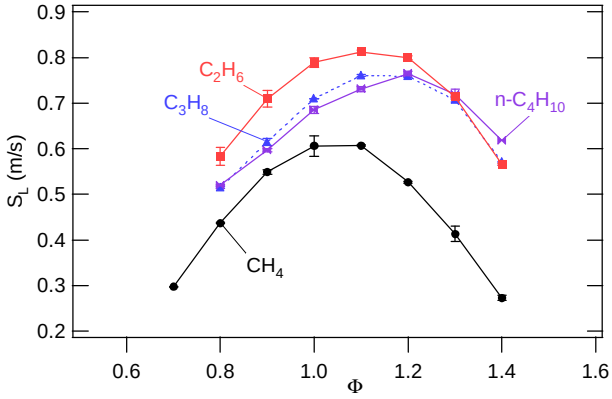


Figure 7: Laminar burning velocity measurements for methane, ethane, propane, and n-butane at T=450 K and P=304 kPa.

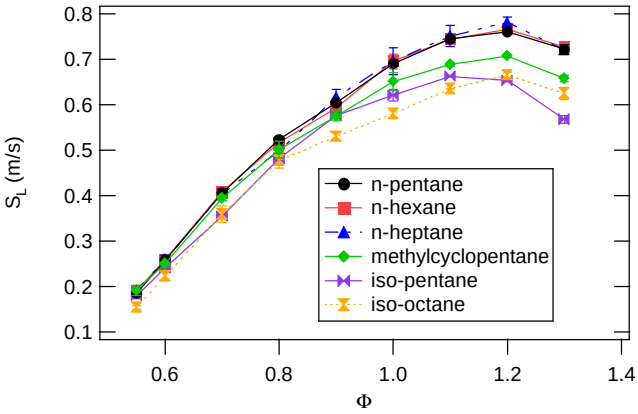


Figure 8: Laminar burning velocities vs. ϕ for several $C_5$-$C_8$ alkanes at T=450 K and P=304 kPa.

the decomposition of the fuel as will be discussed in the following section.

A closer examination of Figure 7 shows that the fuel/air ratio where the peak burning velocity occurs differs for methane through butane. This behavior suggests that stretch effects are not completely absent in our analysis. Because methane has a higher diffusivity than oxygen, preferential diffusion effects at the curved flame front will lead to a Markstein length that increases with increasing ϕ. Physically, this means that lean mixtures are easier to ignite than rich, and that a positively stretched lean (rich) flame such as our outwardly propagating spherical flame will burn faster (slower) than the flame in the planar limit. This serves to shift the peak in the burning velocity curve to leaner equivalence ratios, i.e., to ϕ ~ 1.0-1.1. Conversely, for heavier hydrocarbons the Markstein length decreases with increasing ϕ [8, 20], meaning that rich mixtures are easier to ignite than lean and that that a positively stretched rich (lean) flame will burn faster (slower) than in the planar flame limit. The corresponding maximum is thus shifted to richer conditions, i.e., to near ϕ ~ 1.2. For ethane, which is effectively equidiffusive with oxygen, the peak is near ϕ ~ 1.1. This trend is not specific to the alkanes as it is observed in general for all fuels in this study. These residual stretch effects may also contribute to the differences mentioned earlier for burning velocities determined via pressure rise vs. flame front visualization.

***Alkenes and other small unsaturated species***

The burning velocities of alkenes and alkynes are known to be higher than the corresponding alkanes. This reflects the effects of both higher adiabatic flame temperatures and kinetic pathway differences. Figure 9 shows the burning velocities of ethylene, propylene, allene, 1- and 2-butyne, and 1- and 2-butene. Ethylene is seen to be the fastest, followed by allene, 1-butyne, 2-butyne, and the alkenes. It is interesting to note that the terminal alkyne 1-butyne is appreciably faster

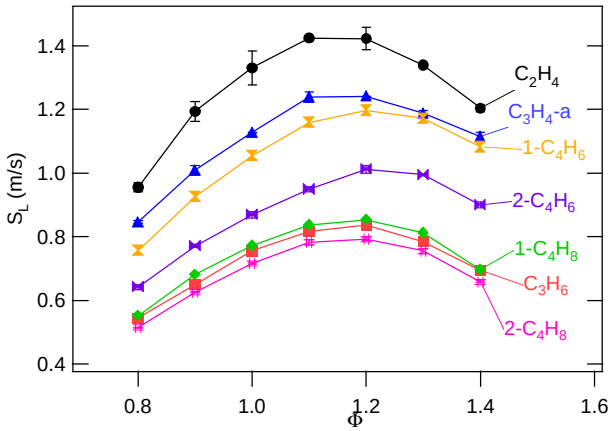


Figure 9: Laminar burning velocities for ethylene, propylene, allene, 1-butyne, and 2-butyne at 450 K and 304 kPa.

than the internal alkyne 2-butyne. This is qualitatively consistent with the shock tube ignition delay measurements of Battin-Leclerc [31] which showed a faster ignition for 1- vs. 2-butyne. The alkene trend discussed below qualitatively mirrors that of the alkanes, i.e., the $C_2$ analogue is fastest, followed by $C_3$, with the $C_4$ and larger alkenes effectively the same. The differences are significantly greater for the alkenes, however; the ratio of the peak burning velocity for ethylene/1-pentene is ~ 1.7 whereas the ratio for ethane/n-pentane is ~ 1.1.

Figure 10 shows data for several $C_5$ alkenes, from which the effect of branching can be discerned. The linear alkenes (1- and 2-pentene) are approximately 10% faster than their branched analogues, which is similar to the spread observed between linear and branched alkane isomers. The effect of cyclization is also similar, with the cyclo-alkene cyclopentene intermediate between the linear and branched $C_5$ alkenes. The data show a small but reproducible benefit for terminal vs. internal double bonds: the data for 1-butene, 1-pentene, and 1-heptene are slightly (4-8 percent) but consistently higher than 2-butene, 2-pentene, and 3-heptene, respectively. The enhancement for terminal vs. internal

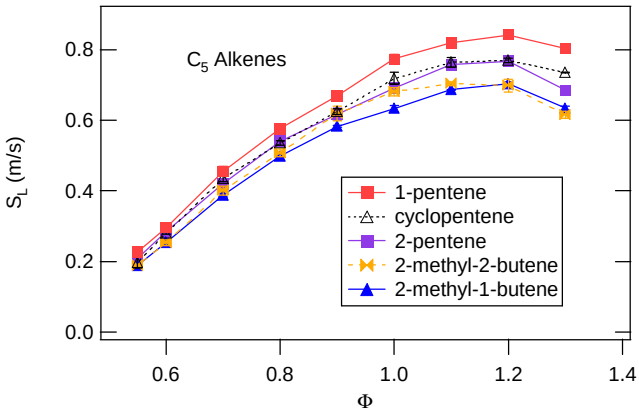


Figure 10: Laminar burning velocities for $C_5$ alkenes at 450 K and 304 kPa.

unsaturation is much lower than identified above for the alkynes.

***Aromatics***

Figure 11 shows that the burning velocity of benzene is approximately 20% faster than toluene, which is consistent with the difference identified by Davis and Law [7] under ambient initial conditions. This decrease upon methyl substitution has been rationalized by the formation of the resonantly stabilized benzyl radical, whose subsequent reactions are expected to be slower than for the species formed during the initial oxidation of benzene. The data for the dimethyl benzenes, i.e., o-, m-, and p- xylene, show a further 10-20% decrease. This decrease is site specific: the burning velocities for o- and p-xylene are nearly equivalent (~10% lower than toluene) while those for m-xylene are slower (~ 20% lower than toluene). The trimethyl benzene data exhibit similar trends - 1,2,4-trimethyl benzene is ~ 5% slower than o- and p-xylene, again demonstrating the burning velocity reduction upon subsequent methyl addition. The data for 1,3,5-trimethyl benzene are effectively the same as for m-xylene and slower than 1,2,4-trimethyl benzene, exhibiting the same site specificity observed for the xylenes. The magnitude of burning velocity reduction upon sequential methyl addition leads to a significant spread for the aromatics; the 50% spread between benzene and m-xylene is larger than the variation between the alkanes and alkenes over the equivalent carbon number range.

The burning velocities for ethyl, propyl, and butyl benzenes are comparable and intermediate between benzene and toluene. These results might be somewhat unexpected since the ethyl and propyl benzenes would be expected to follow a decomposition pathway similar to toluene, i.e., through an initial step involving formation of a resonantly-stabilized radical. Consequently, burning velocities comparable to toluene would be expected. The burning velocities for t-butylbenzene, which are comparable to the ethyl and propylbenzenes, are also somewhat unanticipated. First, there is no benzyl hydrogen present and hence the initial t-butylbenzene decomposition cannot proceed via abstraction to form of resonantly stabilized radical. Second, the alkane and alkene results show that branching with multiple methyl groups leads to a burning velocity reduction; no such reduction is observed for t-butylbenzene vs. ethylbenzene (or iso-propyl vs. n-propylbenzene). The factors contributing to these observations are discussed below.

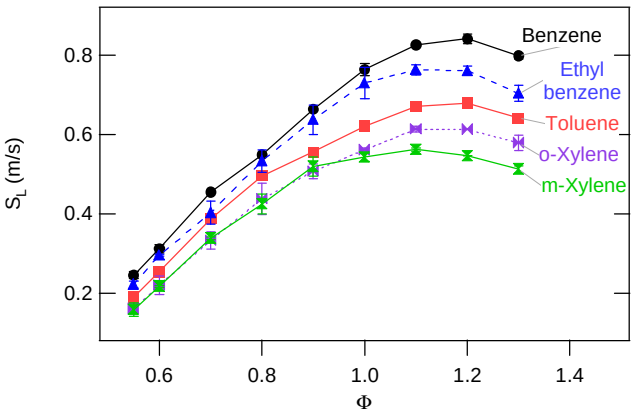


Figure 11: Laminar burning velocity data for several aromatic species at 450 K and 304 kPa.

***Oxygenates***

The burning velocities of three oxygen-containing species have been characterized - ethanol, methyl-t-butyl ether (MTBE), and anisole (methoxy benzene). The data for these species are shown in Figure 12. In general, the burning velocities for the oxygenates are higher than the corresponding alkane, i.e., ethanol is 5-10% higher than ethane and MTBE is comparably higher than the highly branched alkane iso-octane. Similarly, anisole is ~ 20% faster than toluene.

## DISCUSSION

The primary focus of this study is the identification of relative fuel structure effects on laminar burning velocities. Hydrocarbon burning velocities are influenced by both physical and kinetic properties of the mixture. Physical effects are related to factors such as burned and unburned gas temperature, pressure, thermal and mass diffusivity, etc. while the kinetic effects are linked to the chemical species produced during fuel consumption and their ensuing kinetics. The T and P dependence of laminar burning velocity have been discussed in numerous combustion texts [34, 38, 44, 45] and several publications [11, 12, 46, 47]. The present study involves comparisons at the same unburned gas temperature and pressure and hence these factors do not play a role in our analysis of relative fuel effects.

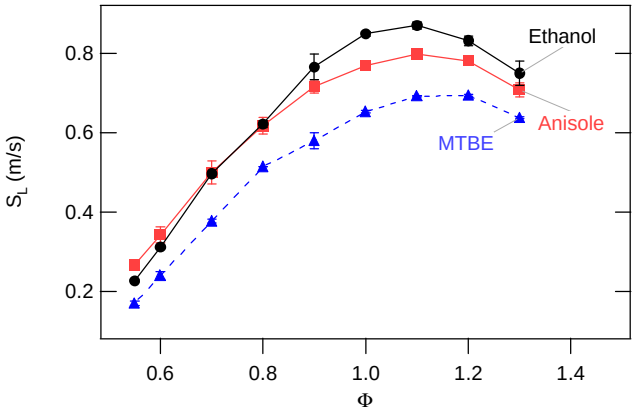


Figure 12: Laminar burning velocity data for the oxygenates ethanol, methyl-t-butyl ether (MTBE), and anisole (methoxy benzene).

Burned gas temperature has long been recognized as having a significant effect on the burning velocity due to its influence on species equilibria and the diffusion of heat/radicals into the flame front. The burned gas temperature is closely related to the mixture's adiabatic flame temperature, and the latter property has often been invoked to explain and predict fuel structure effects on laminar burning velocity [48-50]. Bradley et al. [23] proposed several refinements to established correlations between burning velocity and adiabatic flame temperature in terms of the molar heat of reaction and the volumetric heat release rate. These analyses all point out that these correlations are valid only for fuels of similar structure, and that deviations imply secondary kinetic effects. This is demonstrated in Figure 13a which reproduces data from the study of Davis and Law [7]. It is clear that this correlation is only approximate even for related molecules such as the normal and iso-alkanes. For these molecules, differences in heat capacity, thermal conductivity, and adiabatic flame temperature are small, suggesting that the burning velocity differences primarily reflect kinetic effects. This is further borne out by Figure 13b, which shows laminar burning velocity vs. adiabatic flame temperature for several of the fuels from the present study. It is seen that this correlation is particularly poor for aromatic species and implies a significant contribution from kinetic effects as explained in more detail below.

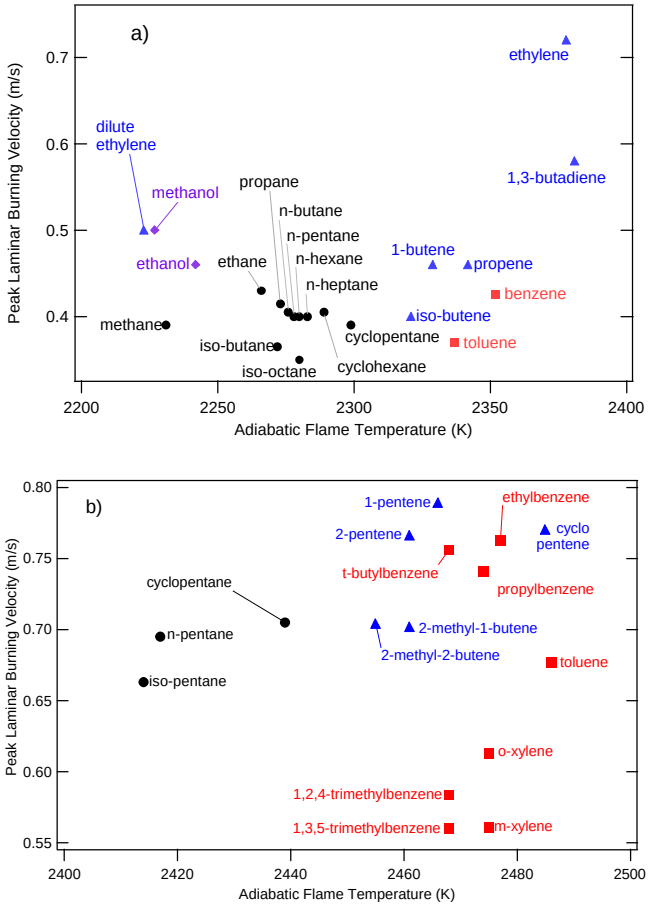


Figure 13: a) Peak laminar burning velocity vs. adiabatic flame temperature from the study of Davis and Law [7] at ambient temperature (300 K) and pressure (101 kPa). b) Peak laminar burning velocity vs. adiabatic flame temperature from the present study. Alkanes are shown in black circles, alkenes and dienes in blue triangles, aromatics in red squares, and oxygenates in purple diamonds.

A modeling approach that has been used extensively to elucidate the effects of kinetics on burning velocity is sensitivity analysis. In this approach, the dependence of the burning velocity on each of the rates in the kinetic mechanism is evaluated. Mathematically, this is represented as

$$S_{i,j} = \frac{\partial \ln A_i}{\partial k_j} \qquad \text{(Eq. 13)}$$

where $S_{i,j}$ is the sensitivity coefficient, $A_i$ is the property of interest (in this case, the burning velocity), and $k_j$ is the rate coefficient for the $j^{th}$ reaction. In practice, sensitivity analyses for most hydrocarbon flames show very similar results, i.e., the most important reactions are not directly fuel specific. For example, Figure 14 shows results from a sensitivity analysis for combustion of methane, ethane, and n-butane at $\phi$=1.0, T=450 K, and P=304 kPa. It can be seen that for all three fuels, the two reactions with the highest sensitivity are $H + O_2 \Leftrightarrow OH + O$ and $OH + CO \Leftrightarrow CO_2 + H$. The former is a critical chain-branching reaction that is vital to establishing the reactive radical pool necessary to support the flame. The latter accounts for a significant fraction of the heat release and thus is linked to increasing the diffusion of heat and radicals into the flame front. The majority of the other reactions primarily involve atomic/molecular hydrogen and oxygen and $C_1/C_2$ hydrocarbons which are common to most hydrocarbon fuels.

While sensitivity analyses are very useful for identifying the specific reactions whose rates play a strong role in influencing the burning velocity, they do not readily provide information on the reactive pathways for conversion of the fuel to combustion products. An alternative approach that does provide this information is that of elemental flux analysis, which tracks the flux of fuel atoms (e.g., C, H) through the reaction paths. We have adopted this technique, in conjunction with sensitivity analyses where appropriate, to derive insight into fuel structure effects on burning velocity as is discussed in the next section. We note that a detailed kinetic analysis for the numerous fuels investigated is well beyond the scope of this report. Thus, only key features are highlighted.

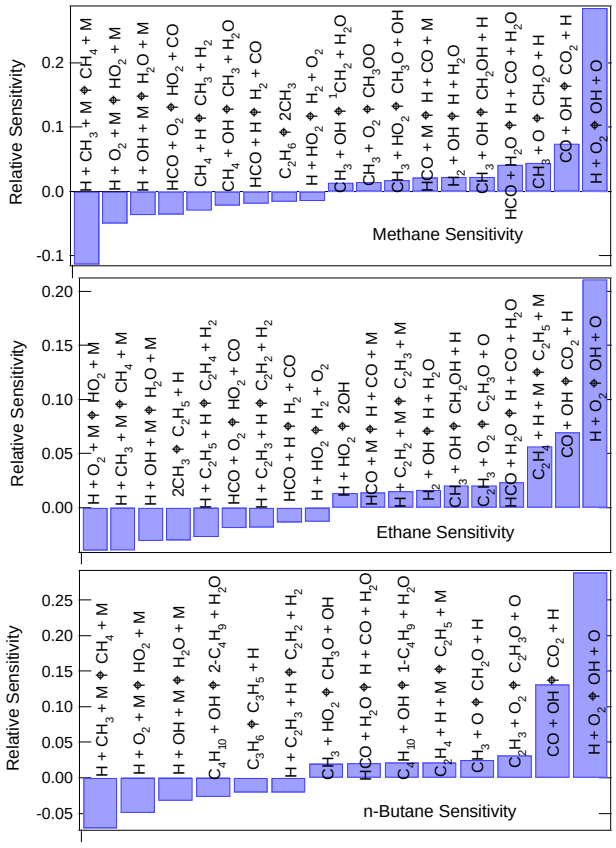


Figure 14: Burning velocity sensitivity analyses for methane, ethane, and n-butane combustion at T=450 K and P = 304 kPa

***Alkanes***

The peak laminar burning velocities of most of the fuels investigated in this study are displayed in Figure 15. The fastest burning fuels, i.e., ethylene, allene, propylene, 1-butyne, and 2-butyne, are omitted for graphical clarity. The left-most column shows that methane is the slowest alkane, while ethane is the fastest. The remaining alkanes fall in between these two. This ranking is consistent with previous literature investigations and ignition delay times at temperatures commensurate with the reaction zone temperature, i.e., 1500 K [51].

A detailed comparison of the methane vs. ethane kinetics forms a useful framework for understanding fuel structure effects for alkanes. The combustion chemistry of methane has been extensively studied [27,28,52] and the overall features of the reaction kinetics associated with methane's laminar burning velocity have been previously discussed [45]. The methane conversion pathways determined from the elemental carbon flux analysis are shown in Figure 16 using the GRI 2.1 mechanism [25] and an internally developed ExxonMobil (EM) mechanism [53]. The flux analysis was applied to the output of a stoichiometric flame calculation using the Sandia PREMIX code [42]. The overall agreement between the two mechanisms is quite good.

It is worth making several points about the flux analysis results in figure 16 and the figures that follow: i) the numbers above the arrows connecting two species represent the fraction of the original carbon that directly connects the two species, ii) not all species and reaction pathways are shown, iii) numbers leaving a species that are larger than the cumulative total into the species reflects the omission of species/reactions mentioned in point ii) above. For example, Figure 16 shows that both the GRI and EMRE mechanism predict that effectively all the methane initially reacts to form methyl radical ($CH_3$). The GRI mechanism predicts that 33% of the original carbon reacts to form formaldehyde ($CH_2O$), while the EMRE mechanism predicts 59%. Many other pathways also produce formaldehyde, with the net effect that 70-80% of the original carbon funnels through $CH_2O$. The combustion if methane is completed by conversion of the $CH_2O$ to HCO, CO, and ultimately $CO_2$.

A closer look at Figure 16 shows that while the sole important decomposition pathway for methane is through the methyl radical via H abstraction, several reaction paths play a role in converting $CH_3$ to products. The three main pathways proceed via formation of ethane, methylene, or formaldehyde. The latter two channels both lead to HCO, followed by CO and ultimately $CO_2$ formation. As pointed out by Westbrook and Dryer [28], methane oxidation is slow compared to other light hydrocarbons as a result of the very low reactivity of methyl radicals. This low reactivity is also manifested as an appreciable amount of ethane formed from methyl recombination, since the low concentrations of radicals typically favor radical-molecule reactions over the statistically less frequent radical-radical reactions.

Another distinguishing feature of methyl radical oxidation is the absence of decomposition pathways that generate H atoms. The high sensitivity of the burning velocity to H atom concentrations is well known from flame inhibition studies [54], and chemical inhibitor efficacy is linked to its ability to divert reactive flux away from the $H+O_2 \rightarrow OH+O$ chain branching reaction into less reactive channels. Thus, decomposition pathways that generate H atoms or other chain branching agents can be expected to accelerate the burning velocity.

The oxidation of ethane demonstrates this point. Results from a carbon flux analysis for ethane using the EM mechanism are shown in Figure 17. Most of the flux proceeds through ethyl radical (99%) to ethylene (71%). Under flame conditions, the ethyl radical rapidly

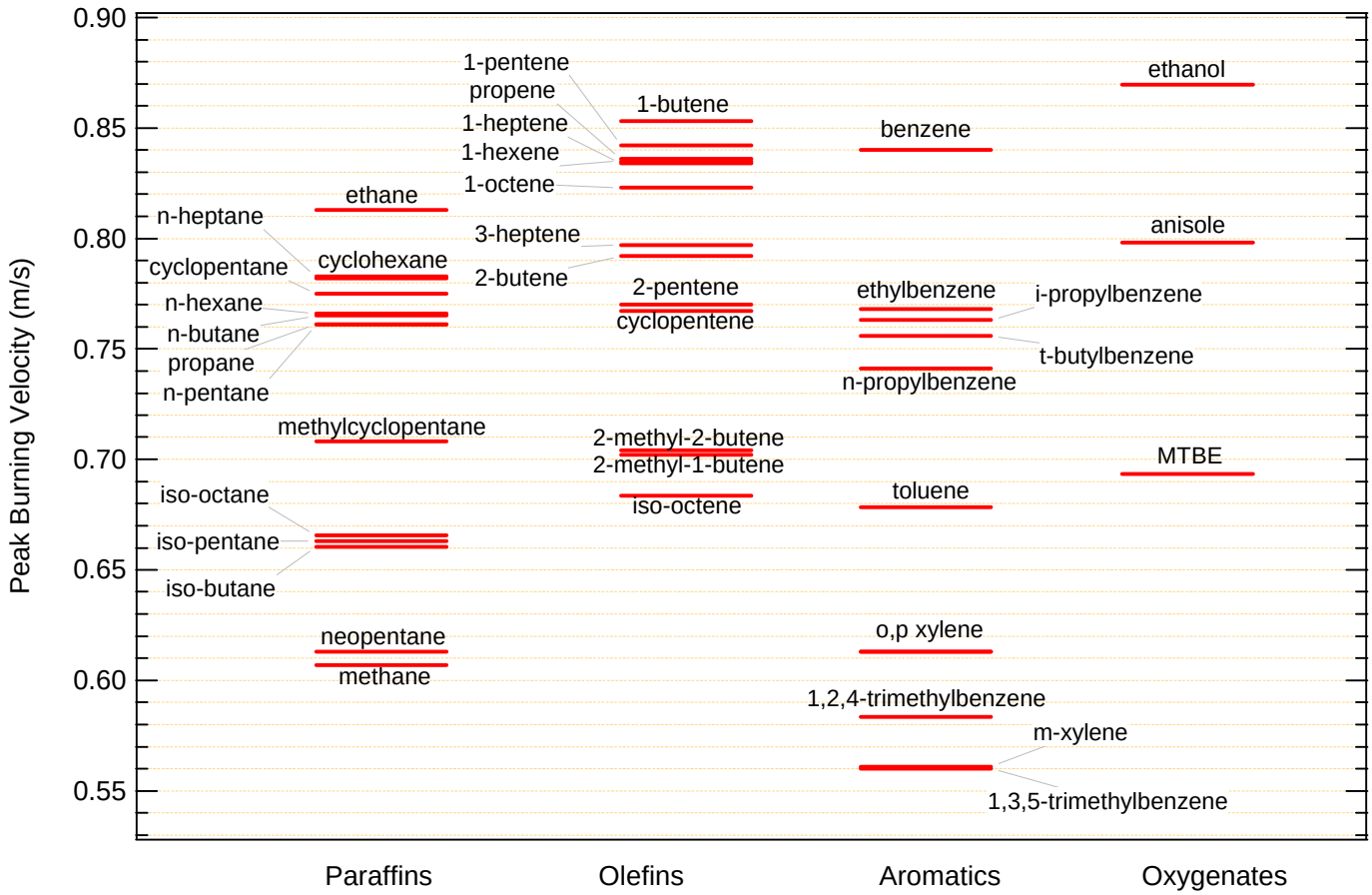


Figure 15. Peak burning velocities for most of the fuels investigated in the present study. The fastest burning fuels ethylene, allene, 1-butyne, and 2-butyne are not included in this figure.

decomposes unimolecularly to form ethylene + H, the latter of which can undergo chain branching with $O_2$. Most of the ethylene proceeds through vinyl radical ($C_2H_3$), which also undergoes chain branching reactions with $O_2$ to form vinoxy + O:

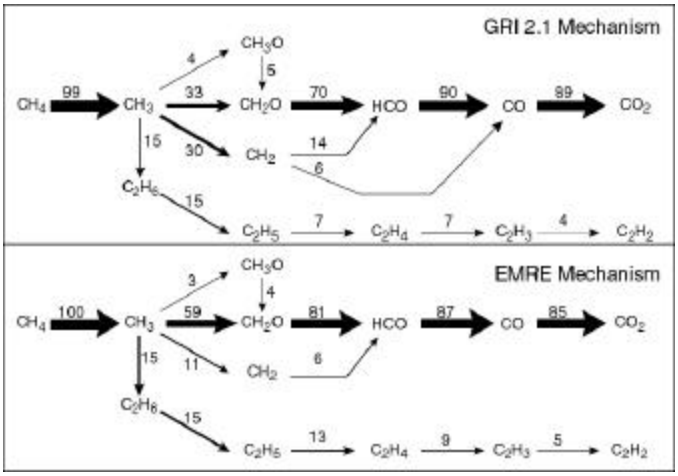


Figure 16: Methane oxidation pathways determined from an elemental carbon flux analysis of the GRI 2.1 mechanism [25] and the EMRE mechanism [53] based on the output from the Sandia PREMIX code [42].

$$C_2H_3 + O_2 \rightarrow C_2H_3O + O \qquad \text{(Eq. 14)}$$

The ethane sensitivity analysis shown in Figure 14 shows that the $H + O_2 \Leftrightarrow OH + O$ and $C_2H_3 + O_2$ reaction (Eq. 14) have a strong positive effect on the burning velocity. Thus, a principle reason that the burning velocity for ethane is fast compared to methane is due to the prominence of fuel decomposition pathways that promote chain branching.

Extension of the carbon flux analyses to larger hydrocarbons helps to elucidate the reasons for the burning velocity reduction with branched vs. normal alkanes. Figure 17 shows flux analysis results for n- and iso-butane oxidation at 1500 K, 101 kPa, and $\phi$=1.0. Oxidation of both isomers is initiated by H abstraction. For n-butane, nearly half of the fuel forms the 1-butyl radical which undergoes β-scission to form ethylene and ethyl. As discussed above, these species decompose through predominantly chain branching pathways which serve to accelerate combustion. The other half goes through 2-butyl radical, which decomposes via β-scission into methyl and propylene. In contrast, nearly three quarters of the iso-butane molecules pass through either iso-propyl or the $(CH_3)_2CH_2$-$CH_2$• radical on the

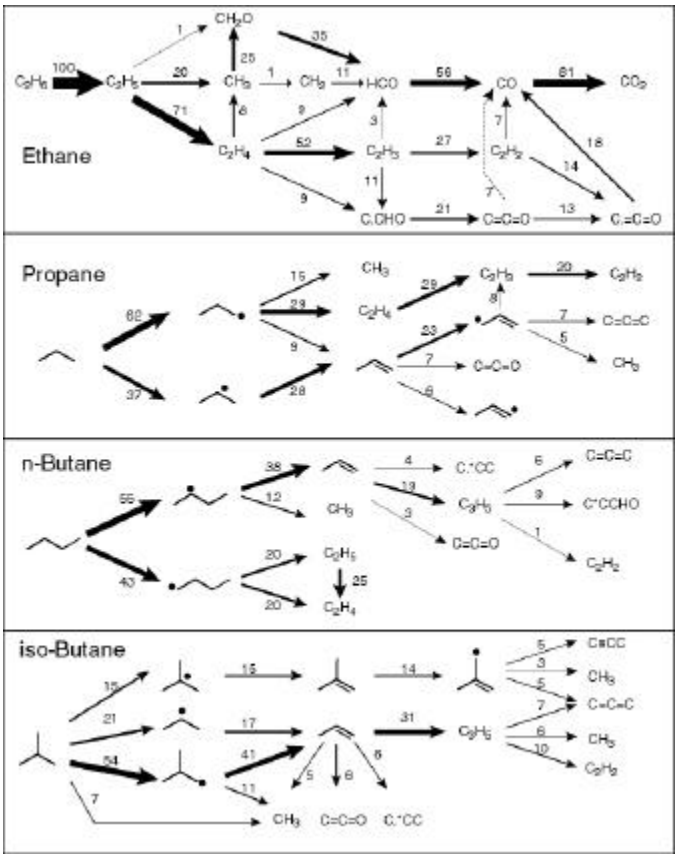


Figure 17: Elemental carbon flux analyses for ethane, propane, n-butane, and iso-butane. The ethane and propane results are calculated from the output of 1-D laminar flame code and the $C_4H_{10}$ results are calculated from the output from a 0-D plug flow reactor code (see text for more details) at T=1500 K and P=101 kPa. The thickness of the pathway lines is proportional to the elemental carbon flux.

way to propylene. In the process, a significant amount of methyl radicals is formed. As discussed above, the oxidation of methyl radicals is relatively slow. Propylene yields primarily allyl radical and a host of smaller molecules, which also decompose via methyl elimination.

The flux analysis shows that 44% of the total carbon atom flux for iso-butane oxidation passes through methyl radical channels. By comparison, the fraction for n-butane is 27%, i.e., about a factor of 2 smaller. Thus, the higher burning velocity of n- vs. iso-butane can be partly attributed to the smaller fraction of n-butane carbon atoms that form methyl radicals, and correspondingly, the larger proportion of molecules that decompose into $C_2$ fragments. The burning velocity sensitivity analysis in Figure 14 is consistent with this latter point as evident by the large sensitivity to the vinyl + oxygen reaction. Flux analyses for larger iso- and n-alkanes show qualitatively similar behavior. For example, results for n-hexane shown in Figure 18 are very similar to the n-butane results. Consequently, the

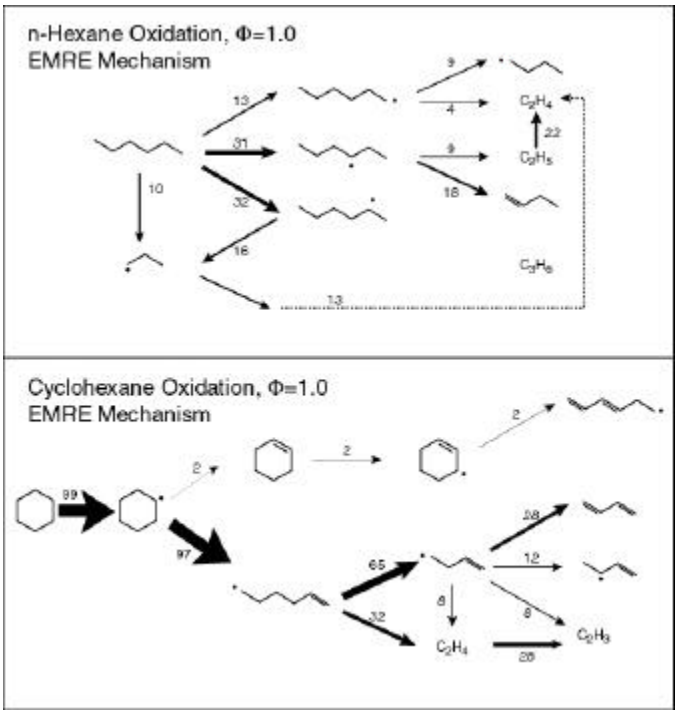


Figure 18: Elemental flux analysis for n-hexane and cyclohexane using the EM kinetic mechanism [53] and a plug flow reactor model at T=1500 K and P=101 kPa.

kinetic factors responsible for the burning velocity differences between n- and iso-alkanes include the fraction of decomposition products that produce methyl vs. $C_2$ fragments.

An analogous situation holds for cycloalkanes as shown for cyclohexane in Figure 18. Following initial hydrogen abstraction, the majority of cyclohexyl molecules undergo ring opening to form a linear radical, a pathway which is entropically favored over the β-scission pathway yielding the cyclo-alkene. Subsequent decomposition reactions yield primarily $C_2$ fragments. This is similar to the behavior of n-alkanes and is the reason that the burning velocity of cycloalkanes are comparable. Based on the analysis above, methyl addition would be expected to lower the burning velocity as observed experimentally due to increased formation of methyl radicals upon fuel decomposition.

***Alkenes***

The kinetic arguments invoked to explain fuel structure effects on alkane burning velocities can also be applied to alkenes. The same qualitative trends are observed: linear alkenes are faster than branched alkenes, and cyclo-alkenes are comparable to linear alkenes. As with the alkanes, the $C_2$ analogue (ethylene) has the fastest burning velocity, although the magnitude of the enhancement (~70%) is much higher than with the alkanes (~10%). Part of the difference can be attributed to the higher adiabatic flame temperature of ethylene. To

address this, Davis and Law [7] carried out burning velocity measurements of a nitrogen-diluted ethylene/air mixture whose adiabatic flame temperature was comparable to undiluted methane/air. The burning velocity of this diluted mixture is 30% lower than the undiluted ethylene/air mixture, but still ~ 25% higher than for methane/air and ~ 20% higher than ethane/air, demonstrating the prominent role of kinetic effects.

Figure 19 shows an elemental flux analysis for ethylene from a premixed laminar flame calculation using the ExxonMobil mechanism [53]. As discussed above for ethane, an appreciable fraction of the ethylene is predicted to decompose through pathways that lead to chain branching, including O and H atom production channels:

$C_2H_3 + O_2 \rightarrow C_2H_3O + O$ (Eq. 15)

$HCO + M \rightarrow H + CO + M$ (Eq. 16)

$\cdot CH_2\text{-}CHO \rightarrow H + C{=}C{=}O$ (Eq. 17)

The prominence of these chain branching pathways leads to accelerated fuel conversion and a higher laminar burning velocity.

The kinetic differences between the larger alkenes and their corresponding alkanes naturally center on reactions of the unsaturated bond. Like the alkanes, abstraction reactions play a prominent role in alkene degradation. A key difference is the low bond strength of the allylic C-H bonds, which are lower than alkane C-H bond strengths and reflect the stability of the resonantly stabilized radical. This leads to a higher propensity to abstract the allylic hydrogens, potentially simplifying the kinetics. Minetti et al. have shown however, that abstraction of both paraffinic and olefinic hydrogens must be considered in describing product formation from the low temperature oxidation of 1-pentene [55]. This consideration is likely more valid at the higher temperatures of flames.

The alkene double bond also gives rise to important competing pathways not present with alkanes, i.e., radical addition to the unsaturated bond. In particular, O

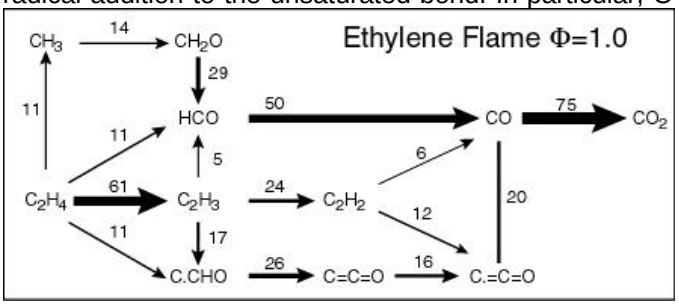


Figure 19: Elemental carbon flux analyses for ethylene using the ExxonMobil mechanism [53] based on the output from the Sandia PREMIX code [42].

atom reactions with olefins are quite facile, as they are with other systems having π-bonded networks. Leppard [56] has shown that radical-addition reactions are primarily responsible for the reactivity differences of alkanes and alkenes under engine autoignition (knocking) conditions. Furthermore, this pathway has been identified as responsible for the key differences in n-pentane vs. 1-pentene autoignition chemistry in rapid compression machine experiments [55].

It is worth noting, however, the fundamental differences between autoignition reactivity and burning velocity behavior of the alkanes and alkenes. The autoignition reactivity as measured by ignition delay times and RON varies significantly with degree of branching and chain length. The burning velocity data similarly show a sensitivity to branching but are largely insensitive to chain length for $C_3$ and larger fuels. Figure 20 shows carbon flux analysis results for 1-butene and 2-butene. In contrast to the n-butane pathway shown in Figure 17, a significant fraction of the olefins resist carbon-carbon bond fragmentation and instead degrade by successive hydrogen elimination to form highly unsaturated hydrocarbons. Consistent with our discussion thus far, this provides more H atoms for chain branching and a corresponding boost in burning velocity.

Perhaps surprisingly, few data have been reported for alkenes in the gasoline boiling range, and detailed mechanisms have been presented for only a few prototypical alkenes [57-60]. Heyberger et al. [60] have constructed a mechanism for 1-butene oxidation which reproduces experimental species profiles and ignition delays. Their flux analysis shows pathways qualitatively similar to those in Figure 20. Moreover, Heyberger et al. note that there is significant flux for the 1,3-butadiene formation channel following metathesis of 1-butene and

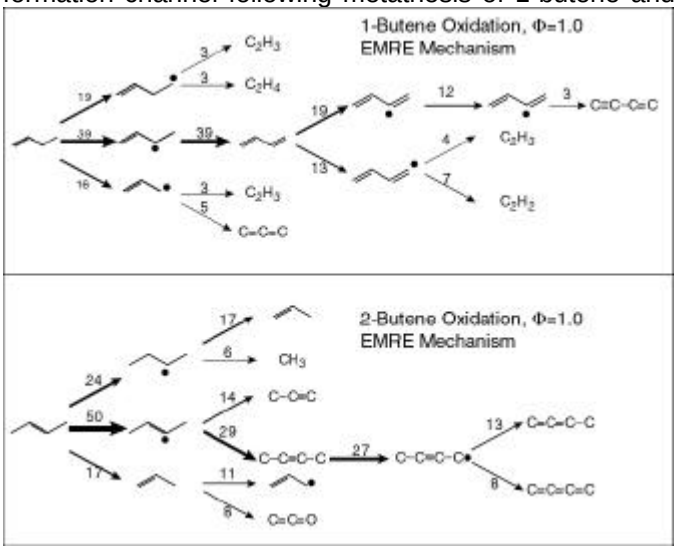


Figure 20: Elemental carbon flux analyses for 1-butene and 2-butene using the ExxonMobil mechanism [53] and a plug flow reactor model at T=1500 K and P=101 kPa.

H loss either via elimination or reaction with $O_2$. Another pathway with significant flux and H atom production results from $O_2$ addition to the resonance stabilized radical formed from abstraction of 1-butene, which give peroxy radicals that decompose to form acetaldehyde and $\bullet CH_2$-CHO, the latter of which decompose to form H + ketene (reaction 17). These types of pathways are not important for alkane decomposition and together with slightly higher burned gas temperatures may explain the higher burning velocities for alkenes vs. alkanes.

While not considered in detail in the present study, the kinetic principles governing the burning velocities of highly unsaturated species such as 1-butyne and 2-butyne can be examined. Battin-Leclerc [31] carried out flux analyses for each isomer under shock tube oxidation conditions (T=1200-1300 K, P=800-900 kPa). Her results show a greater propensity for $C_2$ species formation with 1-butyne vs. 2-butyne, which together with the higher burning velocity for 1-butyne directionally supports the trends identified for alkane and alkene burning velocities.

***Aromatics***

Discussions of aromatic burning velocities in the literature have mostly been limited to benzene and toluene, since few data are available for other aromatics. The lower burning velocity for toluene has been attributed to the formation of the resonantly stabilized benzyl radical upon initial radical attack of the fuel. The higher stability and hence reduced reactivity of resonantly stabilized radicals has been suggested to lead to a slower oxidative degradation of the fuel, and thus a lower burning velocity [7].

Figure 21 shows carbon flux analyses for benzene and toluene using the kinetic mechanism of Bozzelli and coworkers [61-65]. Benzene destruction is predicted to proceed primarily via two paths: abstraction to yield phenyl and O atom addition. Both paths lead through phenoxy, which leads to cyclopentadienyl via CO elimination. This scheme is in qualitative agreement with laboratory flame measurements and modeling which also show these two pathways to be primary benzene destruction routes [66]. The majority of the toluene (~80%) is indeed predicted to pass through benzyl, and many steps are involved in the oxidation of the side chain. Although the majority of the reactive flux for both benzene and toluene is predicted to pass through cyclopentadienyl radical, many more reactions are required for toluene. In contrast, oxidation of benzene to cyclopentadienyl requires fewer steps involving no resonantly stabilized species, leading to faster fuel consumption.

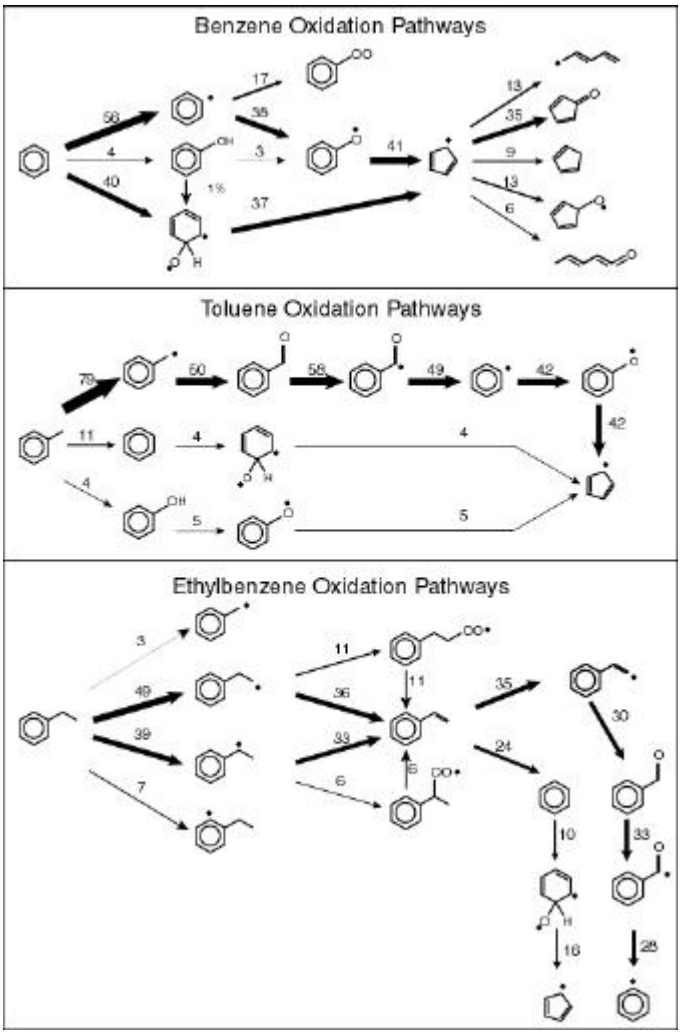


Figure 21. Oxidation pathways for benzene, toluene, and ethylbenzene based on the output of a 0-D plug flow oxidation at 1500 K and 101 kPa using the mechanism of Bozzelli and coworkers [61-65]

Extension of this argument to the larger alkyl aromatics included in this study qualitatively explains the present results. All the aromatic molecules (except t-butylbenzene) have weakly bound benzylic hydrogens and thus form resonantly stabilized radicals following abstraction of this hydrogen. Even though t-butylbenzene does not have a benzylic hydrogen, the unimolecular elimination of methyl radical to form a benzylic radical is expected to be facile at the > 1200 K temperatures commensurate with the preheat zone. Thus, the slower burning velocities of the alkyl benzenes investigated in this study are consistent with the slower oxidation kinetics of resonantly stabilized benzylic radicals.

The ~ 15% slower burning velocity of toluene vs. the other mono-substituted alkyl benzenes can be understood through comparison with other studies of aromatic oxidation. Flow reactor studies of aromatic oxidation have indicated that alkyl benzene consumption

occurs primarily through side chain oxidation, after which aromatic ring oxidation is well described by benzene reactions. These results suggest that the initial oxidation reactions of alkyl benzenes can be considered analogous to those for the corresponding alkane [67-71]. This observation provides a simple framework for rationalizing alkylbenzene kinetics. For example, reactions of alkylbenzene oxidation intermediates such as benzyl radical and styrene can be considered analogous to those of alkane reaction intermediates such as methyl and ethylene, respectively.

The present results are consistent with this description. Ethylbenzene has the fastest burning velocity of the mono alkyl substituted aromatics and toluene the slowest, while ethane is the fastest paraffin and methane the slowest of the fuels in this study. The abstraction reactions of methane and toluene yield relatively unreactive radicals, accounting for their lower burning velocity. Bozzelli et al. have developed a kinetic mechanism for ethylbenzene [65], and a flux analysis based on this mechanism predicts the decomposition pathways shown in Figure 21. By analogy with ethane, H abstraction from ethylbenzene is predicted to be followed by H elimination to form styrene. Furthermore, styrene has been shown to decompose via routes that form phenyl + vinyl [68]. Vinyl formation, together with the preceding H elimination, would accelerate fuel decomposition, yielding an elevated burning velocity for ethylbenzene as is observed with ethane.

Consideration of alkane burning velocities leads to the prediction ethylbenzene > propylbenzene > iso-propyl benzene ~ t-butylbenzene. While ethylbenzene is marginally faster according to Figure 15, the burning velocities of these species can be considered effectively comparable within experimental error. For n-propyl and isopropyl benzene, abstraction will occur from both primary and secondary/tertiary C-H bonds, yielding a mixture of radical intermediates that can further react via β-scission. Dagaut et al. [72] have carried out an experimental and kinetic modeling study of n-propylbenzene oxidation in a jet-stirred reactor and determined that the major pathways for fuel consumption involve either abstraction to form phenylpropyl radical or decomposition to benzyl + $C_2H_5$. Phenylpropyl decomposes unimolecularly to form methyl + styrene, the latter which yields phenyl + $C_2H_4$. Production of the $C_2$ species would be expected to enhance the burning velocity. Alternatively, Litzinger et al. [69] have determined that phenyl shift isomerization pathways are required to explain their propylbenzene flow reactor data. This isomerization pathway is also available following primary hydrogen abstraction of t-butylbenzene, yielding the $(C_6H_5)$-$CH_2$-C•$(CH3)_2$ radical. It is not clear, however, whether these pathways are important for describing the laminar burning velocity of these fuels. It is hoped that the present data may be useful targets for initial mechanism construction due to the high sensitivity of the burning velocity to the initial decomposition pathways.

Another interesting observation from the present study is the regioselectivity of the burning velocities for the xylenes. o- and p-xylene have comparable burning velocities that are ~ 10% higher than m-xylene. This regioselectivity is also exhibited in the trimethylbenzene burning velocities: the o,p isomer 1,2,4 trimethylbenzene is ~ 10% faster than the m- isomer 1,3,5-trimethylbenzene. Lower temperature oxidation studies of the xylene isomers have shown that o-xylene is the most reactive, followed by p- and then m-xylene [73-74]. The higher reactivity of the ortho isomer has been attributed to participation of the adjacent methyl group. In particular, flow reactor oxidation studies at 1150 K have identified the importance of the isomerization pathway that converts o-xylylene to styrene [74], which has been shown to occur unimolecularly [75]. The styrene rapidly decomposes to form phenyl / benzyl + vinyl, the latter of which also promotes chain branching.

Based on these results, the near equivalence of the o- and p-xylene burning velocities is interesting and worth contemplating. The initial radical attack of each xylene isomer forms a resonantly stabilized methylbenzyl radical. As shown in Figure 22, a unimolecular decomposition pathway is available to o- and p-xylene that generates xylylene (bis(methylene) cyclohexadiene) and an H atom. The former have been observed as initial oxidation products for o- and p-xylene, respectively [74-76]. The H atoms would participate in chain branching and thus yield a faster burning velocity for o- / p- vs. m-xylene, for which no such pathway exists. Since the o-xylylene isomerization to styrene is fast at 1200 K and expected to be important under flame front conditions, it is not clear why this channel would not lead to an increased burning velocity for o- vs. p-xylene. Gregory et al. [77] however have carried out studies of isotopically labeled xylene isomers in the exhaust of spark ignition (SI) engines. Their data shows evidence for unimolecular formation of styrene from p-xylene, which they postulate proceeds via p-xylylene.

***Oxygenates***

Figure 15 shows that ethanol has a faster burning velocity than ethane, in agreement with previous literature reports [7]. The adiabatic flame temperature of ethanol/air is comparable to ethane/air, indicating that there is a kinetic basis for the difference. Egolfopoulos et al. [78] have developed an ethanol kinetic mechanism developed in part to fit burning velocity data at 101 kPa.

Their analysis indicates that most of the fuel is consumed via the following pathway:

$$C_2H_5OH \xrightarrow{H,O,OH} CH_3CHOH \xrightarrow{+O_2/-HO_2} CH_3CHO \xrightarrow{H,OH} CH_3CO \xrightarrow{M} CH_3 + CO \quad \text{(Eq. 18)}$$

Considering this pathway, the trends identified for alkanes which relate relative burning velocity to initial fuel decomposition species do not suggest an obvious reason for an elevated burning velocity for ethanol vs. ethane. The second most important consumption pathway in the mechanism of Egolfopoulos et al. involves radical attack at the primary methyl carbon to yield ·$CH_2CH_2OH$, which unimolecularly decays to ethylene + OH. An appreciable yield of ethylene would serve to accelerate the burning velocity. Moreover, both pyrolysis [79] and oxidation [80] studies have shown that the unimolecular decomposition of ethanol to form water + ethylene is a significant pathway at temperatures near 1000 K. This suggests the possibility that the ethanol flame behaves in part like a diluted ethylene + water flame. Figure 13 shows that at ambient conditions, the burning velocity for ethanol [7] and a diluted ethylene flame [78] are comparable, the latter being ~ 5-10% higher. It is worth investigating whether the relative importance of the ethylene-producing pathways is greater than suggested from previous studies and whether this could quantitatively explain ethanol's burning velocity.

## CONCLUSIONS

Laminar burning velocities have been presented for 45 hydrocarbons under elevated temperature (450 K) and pressure (304 kPa). The data for alkanes and alkenes are qualitatively consistent with previous literature investigations at other temperatures and pressures. The results for aromatics are more comprehensive than most previous reports and show a wide range of variation that is sensitive to the site and degree of alkyl substitution. The kinetic effects of fuel structure have been discussed. The principal results are:

- Among the alkanes studied, methane has the slowest burning velocity and ethane the fastest
- Normal alkanes are faster than iso-alkanes
- Similar burning velocities are obtained for $C_4$ and higher n-alkanes
- Cycloalkanes (cyclopentane and cyclohexane) show burning velocities comparable to the linear alkanes
- Methyl substitution leads to slower cycloalkanes burning velocities

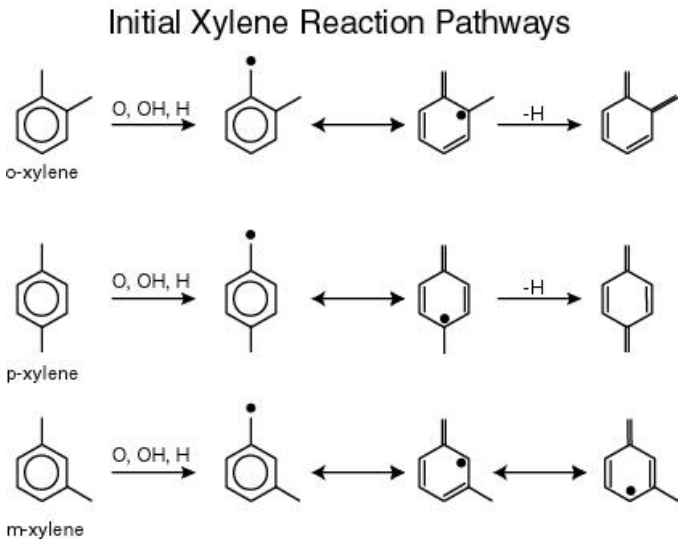


Figure 22: Proposed initial oxidation pathways to explain the faster burning velocities for ortho-, para- vs. meta-xylene

- Alkene burning velocities are faster than those for the corresponding alkane (i.e., one with the same carbon connectivity)
- Highly unsaturated molecules (alkynes, allene) have faster burning velocities than the alkenes, alkanes, and aromatics studies (except ethylene)
- The effects of cyclization and branching on alkene burning velocity is the same as with alkanes
- There is a large (18%) burning velocity benefit for terminal vs. internal triple bonds in linear alkynes; the benefit for terminal vs. internal double bonds in linear alkenes is smaller (~4-8%)
- The kinetic basis for differences in alkene and alkane burning velocity can be related to the extent to which reactive flux channels through channels that produce H atoms (leading to faster burning velocity) vs. methyl radicals (leading to slower burning velocity)
- There is a wide spread in burning velocity for aromatics. Benzene exhibits a burning velocity faster than any of the substituted aromatics
- The slower burning velocities of substituted benzenes can be rationalized by the formation of benzylic intermediates and the resulting slower reactions of these resonantly stabilized radicals
- The faster burning velocities for ethyl, i/n propyl, and t-butylbenzene vs. toluene can be qualitatively rationalized by the presence of unimolecular decomposition pathways of benzylic radicals that

generate H atoms and lead to enhanced chain branching

- Ortho and para substituted xylene and trimethylbenzene exhibit faster burning velocities than the corresponding meta substituted isomer. The presence of H atom elimination pathways with the o,p isomers may explain this regioselectivity

- The limited burning velocity data for oxygenates shows that they are faster than the corresponding non-oxygenated hydrocarbon

- The data and analysis presented in this paper provide a comprehensive, fundamental basis for relating fuel structure effects to combustion efficiency and emissions

The kinetic explanation that pervades this discussion most relates to the extent to which hydrogen atoms are generated during initial decomposition of the fuel. Confirmation that this explanation is general requires confirmation via detailed kinetic modeling, which is dependent on the development of detailed mechanisms. This is particularly valid for aromatics, for which detailed mechanisms are showing great promise in being developed.

## ACKNOWLEDGMENTS

The authors would like to acknowledge Professor Joseph W. Bozzelli for helpful discussions and Dr. Tim Barckholtz for assistance with the kinetic mechanisms and flame calculations.

## REFERENCES

1. T.-W. Kuo, *J. Eng. Gas Turbines Power* 112:348-56 (1990)
2. J.T. Farrell, W. Weissman, R.J. Johnston, J. Nishimura, T. Ueda, and Y. Iwashita, "Fuel Effects on SIDI Efficiency and Emissions", SAE 2003-01-3186
3. M. Gerstein, O. Levine, and E. Wong, "Fundamental Flame Velocities of Hydrocarbons", *Ind. Eng. Chem.*, 43:2770-2 (1951)
4. M. Gerstein, O. Levine, and E. Wong, "Flame Propagation. II. The Determination of Fundamental Burning Velocities of Hydrocarbons by a Revised Tube Method", *J. Am. Chem. Soc.*, 73:418-22 (1951)
5. P. Wagner and G.L. Dugger, "Flame Propagation. V. Structural Influences on Burning Velocity. Comparison of Measured and Calculated Burning Velocity", *J. Am. Chem. Soc.* 77:227-31(1955)
6. G.J. Gibbs and H.F. Calcote, "Effect of Molecular Structure on Burning Velocity", *J. Chem. Eng. Data*, 4(3):226 (1959)
7. S.G. Davis and C.K. Law, "Determination of Fuel Structure Effects on Laminar Flame Speeds of $C_1$ to $C_8$ Hydrocarbons", *Combust. Sci. and Tech.* 140:427-49 (1998)
8. D. Bradley, R.A. Hicks, M. Lawes, C.G.W. Sheppard, and R. Wooley, "The Measurement of Laminar Burning Velocities and Markstein Numbers for Iso-octane-Air and Iso-octane-n-Heptane-Air Mixtures at Elevated Temperatures and Pressures in an Explosion Bomb", *Comb. Flame* 115:126-44 (1998)
9. M.I. Hassan, K.T. Aung, O.C. Kwon, and G.M. Faeth, "Properties of Laminar Premixed Hydrocarbon/Air Flames at Various Pressures", *J. Propulsion and Power*, 14(4):479-88 (1998)
10. K.T. Aung, K.-K Tseng, M.A. Ismail, and G.M. Faeth, "Laminar Burning Velocities and Markstein Numbers of Hydrocarbon/Air Flames", *Comb. Flame* 102:526-30 (1995)
11. S.P. Sharma, D.D. Agrawal, and C.P. Gupta, "The Pressure and Temperature Dependence of Burning Velocity in a Spherical Combustion Bomb", *18th Symp. (Int) Comb.* 493-501 (1981)
12. T. Iijima and T. Takeno, "Effects of Temperature and Pressure on Burning Velocity", *Comb. Flame* 65:35-43 (1986)
13. Y. Dong, C.M. Vagelopoulos, G.R. Spedding, F.N. Egolfopoulos, "Measurement of Laminar Flame Speeds Through Digital Particle Image Velocimetry: Mixtures of Methane and Ethane with Hydrogen, Oxygen, Nitrogen, and Helium" *29th Symp. (Int) Comb.* 1419-26 (2002)
14. M. Metghalchi and J.C. Keck, "Laminar Burning Velocity of Propane-Air Mixtures at High Temperature and Pressure", *Comb. Flame* 38:143-54 (1980)
15. M. Metghalchi and J.C. Keck, "Burning Velocities of Mixtures of Air With Methanol, Isooctane, and Indolene at High Pressure and Temperature", *Comb. Flame* 48:191-210 (1982)
16. D. Bradley, C.G.W. Sheppard, R. Woolley, D.A. Greenhalgh, and R.D. Lockett, "The Development and Structure of Flame Instabilities and Cellularity at Low Markstein Numbers in Explosions", *Comb. Flame* 122:195-209 (2000)
17. X.J. Gu, M.Z. Haq, M. Lawes, and R. Wooley, "Laminar Burning Velocity and Markstein Lengths of Methane-Air Flames", *Comb. Flame* 121:41-58 (2000)
18. G. Rozenchan, D.L. Zhu, C.K. Law, and S. D. Tse "Outward Propagation, Burning Velocities, and Chemical Effects of Methane Flames up to 60 ATM. *29th Symp. (Int) Comb.* 1461-9 (2002)

19. F. Rahim M. Elia, M. Ulinski, and M. Metghalchi, "Burning Velocity Measurements of Methane-Oxygen-Argon Mixtures and an Application to Extend Methane-Air Burning Velocity Measurements", *Int. J. Engine Research* 3:81-92 (2002)
20. R.J. Johnston and J.T. Farrell, "Laminar Burning Velocities and Markstein Lengths Of Aromatics At Elevated Temperature And Pressure", submitted for publication
21. G.E. Andrews and D. Bradley, "Determination of Burning Velocities: A Critical Review", *Comb. Flame* 18:133-53 (1972)
22. C.K. Law, "Dynamics of Stretched Flames", *22nd Symp. (Int) Comb.* 1381-402 (1988)
23. D. Bradley, S. E.-D Habik, and S.A. El-Sherif, "A Generalization of Laminar Burning Velocities and Volumetric Heat Release Rates", *Comb. Flame* 87:336-46 (1991)
24. R.R. Hibbard and B. Pinkel, "Flame Propagation. IV. Correlation of Maximum Fundamental Flame Velocity with Hydrocarbon Structure", *J. Am. Chem. Soc.*, 73:1622-5 (1951)
25. G.P. Smith, D.M. Golden, M. Frenklach, N.W. Moriarty, B. Eiteneer, M. Goldenberg, C.T. Bowman, R.K. Hanson, S. Song, W.C. Gardiner, V.V. Lissianski, and Z. Qin, GRIMECH 2.1, http://www.me.berkeley.edu/gri_mech/
26. Z. Qin, V.V. Lissianski, H. Yang, W.C. Gardiner, S.G. Davis, and H. Wang, "Combustion Chemistry Of Propane: A Case Study Of Detailed Reaction Mechanism Optimization", *28th Symp. (Int) Comb.* 1663-9 (2000)
27. J. Warnatz, "The Structure Of Laminar Alkane, Alkene, And Acetylene Flames", *18th Symp. (Int) Comb.*, 369-84 (1981)
28. C.K. Westbrook and F.L. Dryer, "Chemical Kinetic Modeling of Hydrocarbon Combustion", *Prog. Energy Combust. Sci.*, 10:1-57 (1984)
29. H.J. Curran, W.J. Pitz, C.K. Westbrook, C.V. Callahan, and F.L. Dryer, "Oxidation Of Automotive Primary Reference Fuels At Elevated Pressures", *27th Symp. (Int) Comb.* 379-87 (1998)
30. C.K. Westbrook, W.J. Pitz, H.J. Curran, J. Boercker, E. Kunrath "Chemical Kinetic Modeling Study Of Shock Tube Ignition Of Heptane Isomers" *Int. J. Chem. Kin.,* 33(12): 868-77 (2001)
31. F. Battin-Leclerc, "Development Of Kinetic Models For The Formation And Degradation Of Unsaturated Hydrocarbons At High Temperature", *Phys. Chem. Chem. Phys.* 4(11): 2072-8 (2002)
32. NIST-JANAF Thermochemical Tables, Third edition, Journal of Physical and Chemical Reference Data.
33. J.M. Grenda and J.W. Bozzelli, Manuscript to be submitted to *Computers in Chemistry*
34. R.A. Strehlow, *Combustion Fundamentals*, McGraw-Hill, New York, 1988
35. J.B. Heywood, *Internal Combustion Engine Fundamentals*, McGraw-Hill, New York, 1988
36. J.D. Gabano, T. Kageyama, F. Fisson, and J.C. Leyer, "Experimental Simulation of Engine Knock by Means of a Preheated Static Combustion Chamber", *22nd Symp. (Int) Comb.* 447-54 (1988)
37. D. Bradley, C.G.W. Sheppard, R. Woolley, "Unstable Explosion Flames and Acoustic Oscillations", *Presentation at ICDERS* (2001)
38. B. Lewis and G. von Elbe, *Combustion, Flames and Explosions of Gases*, Academic Press, Orlando, 1987
39. D. Bradley, private communication
40. J. Revel, J.C. Boettner, M. Cathonnet, and J.S. Bachman, "Derivation Of A Global Chemical Kinetic Mechanism For Methane Ignition And Combustion", *J. Journal de Chimie Physique et de Physico-Chimie Biologique*, 91:365-82 (1994)
41. R.J. Kee, F.M. Rupley, E. Meeks, and J. A. Miller, "*CHEMKIN-III: A Fortran Chemical Kinetics Package for the Analysis of Gas-Phase Chemical and Plasma Kinetics",* Sandia Report SAND-96-8216 (1996)
42. R.J. Kee, J.F. Grcar, M.D. Smooke, and J.A. Miller, "*PREMIX: A Fortran Program For Modeling Steady Laminar One-Dimensional Premixed Flames",* Report (1985), SANDIA-85-8240
43. I.P. Androulakis, J.M. Grenda, and J.W. Bozzelli, *J. AIChE*, submitted.
44. R.M. Fristrom, *Flame Structure and Processes*, Oxford University Press, New York, 1995
45. I. Glassman, *Combustion*, Academic Press, San Diego, 1996
46. T.W. Ryan III and S.S. Lestz, "The Laminar Burning Velocity of Isooctane, N-Heptane, Methanol, Methane, and Propane at Elevated Temperature and Pressures in the Presence of a Diluent", *SAE Paper 800103* (1980)
47. D. Lee, J. Shakal, S. Goto, and H. Ishikawa, *SAE Paper 982448* (1998)
48. D.M. Simon, "Flame Propagation. III. Theoretical Consideration Of The Burning Velocities Of Hydrocarbons", *J. Am. Chem. Soc.,* 73:422 (1951)
49. P.L. Walker and C.C. Wright, "Hydrocarbon Burning Velocities Predicted By Thermal Versus Diffusional Mechanisms", *J. Am. Chem. Soc.*, 74:3769 (1952)
50. D. Kretschmer and J. Odgers, "The Prediction of Laminar Flame Speeds for Weak Mixtures", *Transactions of ASME*, 119:566-572 (1997)
51. A. Burcat, K. Scheller, and A. Lifschitz, "Shock Tube Investigation Of Ignition In Ethane-Oxygen-Argon Mixtures", *Comb. Flame.*, 16:29-33 (1971)
52. J.A. Miller, R.J. Kee, and C.K. Westbrook, "Chemical Kinetics and Combustion Modeling", *Annu. Rev. Phys. Chem.*, 41:345-87 (1990)
53. A.Y. Chang, J.W. Bozzelli, and A.M. Dean, "Kinetic Analysis Of Complex Chemical Activation And Unimolecular Dissociation Reactions Using QRRK

Theory And The Modified Strong Collision Approximation", *Zeitschrift für Physikalische Chemie (Muenchen)* 214(11):1533-1568. (2000)
54. V. Babushok, W. Tsang, G.T. Linteris, and D. Reinelt, "Chemical Limits To Flame Inhibition", *Comb. Flame.*, 115:551-60 (1998)
55. R. Minetti, A. Roubaud, E. Therssen, M. Ribaucour, and L.R. Sochet, "The Chemistry Of Pre-Ignition Of N-Pentane And 1-Pentene", *Comb. Flame.*, 118:213-20 (1999)
56. W.R. Leppard, "A Comparison of Olefin and Paraffin Autoignition Chemistries: A Motored-Engine Study", *SAE Paper 892081* (1989)
57. P. Dagaut, M. Cathonnet, and J.C. Boettner, "Experimental Study And Kinetic Modeling Of Propene Oxidation In A Jet Stirred Flow Reactor", *J. Phys Chem* 92:661 (1988)
58. A. Chakir, M. Cathonnet, J.C. Boettner, and F. Gaillard, "Kinetic Study Of 1-Butene Oxidation In A Jet-Stirred Flow Reactor", *22nd Symp. (Int) Comb.* 873 (1988)
59. S.D. Thomas, A. Bhargava, P.R. Westmoreland, R.P. Linstedt, and G. Skevis, "Propene Oxidation Chemistry In Laminar Premixed Flames", *Bull. Soc. Chim. Belg.* 105:501 (1996)
60. B. Heyberger, N. Belmekki, V. Conraud, P.-A. Glaude, R. Fournet, and F. Battin-Leclerc, "Oxidation of Small Alkenes at High Temperature", *Int. J. Chem. Kin.* 34:666-77 (2002)
61. X. Zhong, "Molecular Beam Mass Spectrometry Measurement Of 1-Butene Pyrolysis And Combustion Products: Stable And Active Species Profiles, And, Combustion Modeling Of Benzene, Phenol, Anisole And Cyclopentadiene Thermodynamic Parameters And Elementary Reaction Kinetic Mechanism", Ph.D Thesis Rutgers University Newark, (1998)
62. X. Zhong and J.W. Bozzelli, "Thermochemical And Kinetic Analysis On The Addition Reactions Of H, O, OH, And $HO_2$ With 1,3-Cyclopentadiene", *Int. J. Chem. Kin.* 29:893 (1997)
63. X. Zhong and J.W. Bozzelli, "Thermochemical and Kinetic Analysis of the H, OH, $HO_2$, O, and $O_2$ Association Reactions with Cyclopentadienyl Radical", *J. Phys Chem* 102:3537 (1998)
64. W.J. Pitts, K. Sheshadri, J.W. Bozzelli, X. Zhong, and C.K. Westbrook United States Meeting of the Combustion Inst, Proceedings. (2001)
65. J.W. Bozzelli, private communication.
66. S.G. Davis, H. Wang, K. Brezinsky, and C.K. Law, "Laminar Flame Speeds and Oxidation Kinetics of Benzene-Air and Toluene-Air Flames", *22nd Symp. (Int) Comb.* 1025 (1996)
67. C. Venkat, K. Brezinsky, and I. Glassman, "High-Temperature Oxidation Of Aromatic Hydrocarbons", *19th Symp. (Int) Comb.* 143 (1982)
68. T.A. Litzinger, K. Brezinsky, and I. Glassman, "The Oxidation of Ethylbenzene Near 1060 K", *Comb. Flame.*, 63:251-67 (1986)
69. T.A. Litzinger, K. Brezinsky, and I. Glassman, "Reactions of N-Propylbenzene During Gas Phase Oxidation", *Comb. Sci. and Tech.,* 50:117-33 (1986)
70. K. Brezinsky, G.T. Linteris, T.A. Litzinger, and I. Glassman, "High Temperature Oxidation of N-Alkyl Benzenes", *21st Symp. (Int) Comb.* 833-40 (1986)
71. K. Brezinsky, T.A. Litzinger, and I. Glassman, "The High Temperature Oxidation Of The Methyl Side Chain Of Toluene", *Int. J. Chem. Kin.* 16:1053 (1984)
72. P. Dagaut, A. Ristori, A. El Bakali, and M. Cathonnet, "Experimental And Kinetic Modeling Study of the Oxidation of n-Propylbenzene", *Fuel*, 81:173-84 (2002)
73. A. Roubaud, R. Minetti, L.R. Sochet, "Oxidation and Combustion of Low Alkylbenzenes at High Pressure: Comparative Reactivity and Auto-Ignition", *Comb. Flame.*, 121:535-41 (2000)
74. J.L. Emdee, K. Brezinsky, and I. Glassman, "Oxidation of o-Xylene", *23rd Symp. (Int) Comb.* 77-84 (1990)
75. O.L. Chapman, U.-P.E. Tsou, and J.W. Johnson, "Thermal Isomerization of Benzocyclobutene", *J. Am. Chem. Soc.,* 109:553 (1987)
76. J.L. Emdee, K. Brezinsky, and I. Glassman, "High-Temperature Oxidation Mechanisms of m- and p-Xylene", *J. Phys. Chem.,* 95:1626-35 (1991)
77. D. Gregory, R.A. Jackson, and P.J Bennett, "Mechanisms for the Formation of Exhaust Hydrocarbons in a Single Cylinder Spark-Ignition Engine, Fueld with Deuterium-Labeled ortho-, meta-, and para-xylene", *Comb. Flame.*, 118:459-68 (1999)
78. F.N. Egolfopoulos, D.X. Du, and C.K. Law, "A Study on Ethanol Oxidation Kinetics in Laminar Premixed Flames, Flow Reactors, and Shock Tubes", *24th Symp. (Int) Comb.* 833-41 (1992)
79. J. Li, A. Kazakov, and F.L. Dryer, "Ethanol Pyrolysis Experiments In A Variable Pressure Flow Reactor", *Int. J. Chem. Kin.* 33:859 (2001)
80. N. Marinov, "A Detailed Chemical Kinetic Model For High Temperature Ethanol Oxidation", *Int. J. Chem. Kin.* 31:183 (1999)